Sedimentary Geology 451 (2023) 106409

Contents lists available at ScienceDirect

Sedimentary Geology

journal homepage: www.elsevier.com/locate/sedgeo

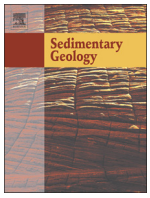

Detrital zircon signals of the late Eocene provenance change of the Pearl River Mouth Basin, northern South China Sea

Yichao Li [a,b], Chenglin Gong [a,b,*], Guangrong Peng [c], Xinwei Qiu [c], Ronald J. Steel [d], Zhangbo Xiao [c], Yanbing He [c], Kun Qi [a,b], Yixin Yu [a,b]

[a] State Key Laboratory of Petroleum Resources and Prospecting, China University of Petroleum (Beijing), Beijing 102249, China
[b] College of Geosciences, China University of Petroleum (Beijing), Beijing 102249, China
[c] Shenzhen Branch of China National Offshore Oil Corporation Ltd, Shenzhen, Guangdong 518052, China
[d] Department of Geological Sciences, Jackson School of Geosciences, University of Texas, Austin, TX 78712, USA

ARTICLE INFO

Article history:
Received 4 February 2023
Received in revised form 17 April 2023
Accepted 18 April 2023
Available online 26 April 2023

Editor: Dr. Brian Jones

Keywords:
Provenance change
Detrital zircon U–Pb age
Crustal thickness
Paleogeographic pattern
Pearl River Mouth Basin

ABSTRACT

A provenance change driven by tectonic and climatic forcing records the surface geodynamic processes, and is of great significance for our understanding of evolving continental margins. The Paleogene succession in the Pearl River Mouth Basin (PRMB), northern South China Sea (SCS), records the variation of sediment-routing systems and thus can reveal provenance changes and their association with the regional paleogeographic evolution on the South China margin. We use U–Pb ages and the Eu/Eu* anomalies of detrital zircons from Paleogene samples in Huizhou Sag, northern PRMB to reconstruct the sediment-routing system and the crustal thickness of the South China margin, respectively. The results show that from the middle Eocene to the upper Eocene there was a rapid increase in proportion of old-age zircon populations (>200 Ma), reflecting a provenance change from the intrabasinal Mesozoic basement to the extrabasinal South China Block. Moreover, the Eu/Eu* anomalies in detrital zircons suggest that during Cretaceous the crustal thickness increased from ca. 40 km to ca. 70 km in the South China margin, corresponding to the uplift of the extensive Coastal Mountains along the South China margin. The substantial rock uplift is believed to be related to the subduction between the Cretaceous Izanagi Plate and the South China Block. A new paleogeographic pattern is reconstructed, where we relate the late Eocene provenance change to the relief generated by the Cretaceous orogenic event. Firstly, due to the rain shadow effect, the uplift of the Coastal Mountains prevented pacific air from reaching into the South China hinterland, causing the northwestern side of the Coastal Mountains to be arid whereas the southeastern side being humid. Then, on the humid southeastern foothills, the paleo-Pearl River originated from the Late Cretaceous to the middle Eocene and transported more and more sediments from the South China Block to PRMB since the late Eocene, causing the provenance change from the intrabasinal basement to extrabasinal South China Block.

1. Introduction

From mountainous environments to the sedimentary basins, tectonic and climatic forcing plays a significant role in the evolution of the paleogeography, and this in turn drives a change of provenance of the whole sedimentary system (Dickinson and Gehrels, 2003; Carter et al., 2010; Armitage et al., 2011; Gilmullina et al., 2022). The provenance change of a source-to-sink system, therefore, documents the surface geodynamic processes and is of great significance for our understanding on the evolution of continental margins (Allen, 2008; Galloway et al., 2011; Bradley and O'Sullivan, 2017; Cao et al., 2018).

Despite being a minor component of clastic sedimentary rocks, detrital zircon plays a significant role in sediment provenance analysis and in crustal evolution studies due to their physiochemical resilience and high concentrations of certain key trace elements (Cawood et al., 2012). As the most common method in provenance analysis, detrital zircon U–Pb geochronology has long been used in reconstructing of sediment-routing systems. Additionally, recent research found that zircon Eu anomaly positively correlates with crustal thickness (Tang et al., 2021), and has received more attention in quantitative constraints on past crustal thickness (Brudner et al., 2022; Carrapa et al., 2022; Chen et al., 2022; Liu et al., 2023).

The northern continental margin of the South China Sea (SCS), located at the conjunction of Pacific, Eurasian and Indo-Australian plates, went through complex tectonic evolution since the Late Mesozoic (Taylor and Hayes, 1983; Northrup et al., 1995; Li et al., 2018).

* Corresponding author at: College of Geosciences, China University of Petroleum (Beijing), Beijing 102249, China.
E-mail address: chenglingong@cup.edu.cn (C. Gong).

https://doi.org/10.1016/j.sedgeo.2023.106409
0037-0738/

Accordingly, the Pearl River Mouth Basin (PRMB), one of the continental margin basins on the northern SCS, belonged to the rift lacustrine environment during Eocene and early Oligocene, whereas since late Oligocene it was dominated by the post-rift marine environment. Through provenance analysis, previous studies found that the Paleogene PRMB was successively fed by two main provenances, the intrabasinal uplifts and fault blocks of the basement and the extrabasinal drainage system, and it was speculated that the timing of that provenance change from intrabasinal to extrabasinal is Eocene–Oligocene (Shao et al., 2016, 2019; Wang et al., 2017, 2019; Ma et al., 2019; Zeng et al., 2019). However, due to the great depth of burial and the limited sampling of the Paleogene succession, it has been difficult to constrain the specific timing of active change between the two catchment regions. Moreover, the cause and mechanism behind the provenance change of the Paleogene PRMB are still unclear. Previous studies indicated that the provenance change is related to the rift evolution within PRMB (Wang et al., 2017). But now more and more evidences suggest that the provenance change occurred earlier than the rift ending in northern PRMB. Therefore, environmental forcings that have influence over relatively larger areas may drive the provenance change and thus need to be considered. The genetic linkages among (1) occurrence of provenance change, (2) evolution of the paleogeographic pattern, and (3) tectonic and climatic forcings on the northern continental margin of SCS will be further investigated herein.

In this study, we focus on the U–Pb ages and the Eu/Eu* anomalies of detrital zircons from Paleogene sandstones in the northern PRMB. We (1) determine the Paleogene provenance change of northern PRMB according to the cumulative age distribution (CAD) plots, the kernel density estimate (KDE) plots, and the multidimensional scaling (MDS) plots of U–Pb ages, (2) reconstruct the crustal thickness of the South China margin and the associated tectonic background based on the Eu/Eu* anomalies, and finally (3) investigate the cause of the observed provenance change of the PRMB through a comprehensive analysis of the paleogeographic pattern on South China margin.

2. Geological setting

2.1. Tectono-stratigraphic evolution of the Paleogene PRMB

As one of the most important sedimentary basins in the northern SCS, PRMB experienced several major tectonic events during the Cenozoic, resulting in different depositional environments coupled with magmatic rocks (Figs. 1 and 2). During the Paleogene, the tectono-stratigraphic evolution of PRMB can be divided into pre-rift, syn-rift, and transitional stages

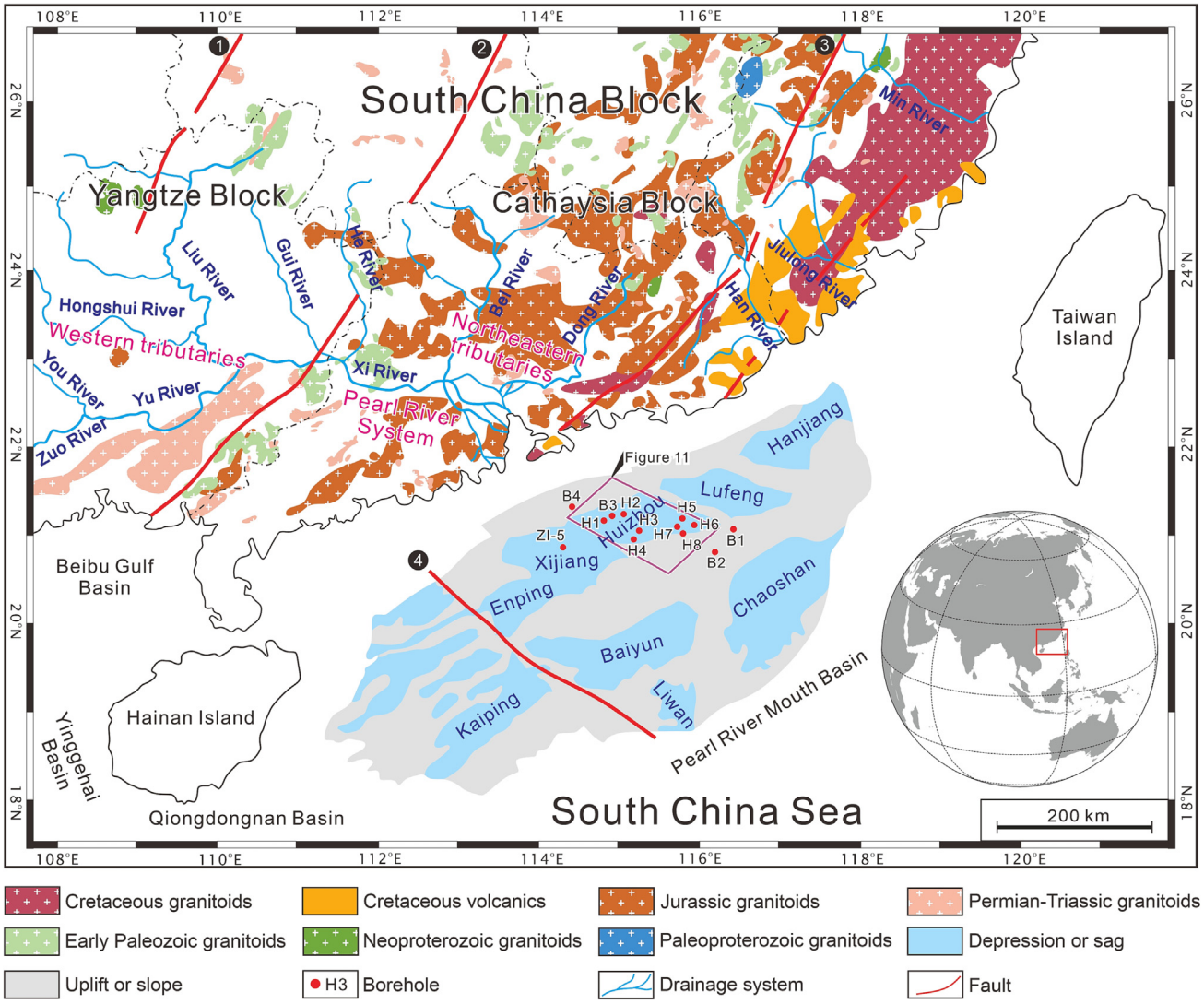

Fig. 1. Regional map of the northern South China Sea (SCS) showing details of the Pearl River Mouth Basin (PRMB) and its potential source areas (modified from Wang et al., 2018). The study area is marked by the red polygon, within which map-view locations of borehole data used in this study are also shown.

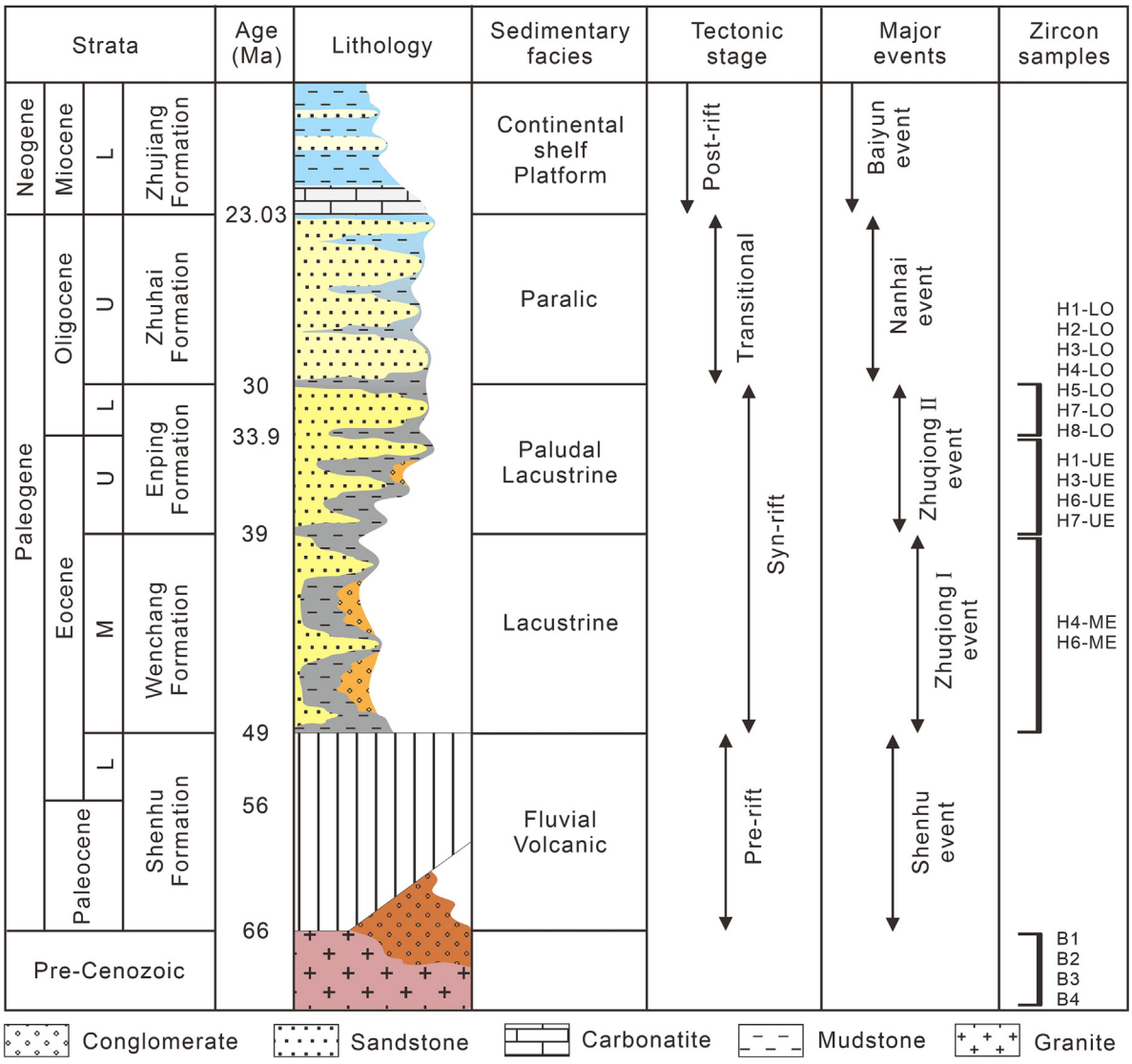

Fig. 2. Schematic stratigraphic column of the Paleogene PRMB showing its lithologic characteristics (Wang et al., 2018), sedimentary facies (Wang et al., 2017), and tectonic evolution (Taylor and Hayes, 1983; Shao et al., 2019). Locations of zircon samples in this study are also labeled. L: lower; M: middle; U: upper.

(Fig. 2) (Yu, 1994). The volcanic and sedimentary rocks of the Paleocene to lower Eocene Shenhu Formation, which were formed during the pre-rift stage dominated by the Shenhu event, are absent in PRMB. During the middle Eocene to early Oligocene syn-rift stage, the PRMB experienced two episodes of the Zhuqiong event, including the Zhuqiong I and II events (Wang et al., 2020). The Zhuqiong I event occurred during middle Eocene and occurred within lacustrine and fluvial deposits of middle Eocene Wenchang Formation; the Zhuqiong II event occurred from late Eocene to early Oligocene and occurred within deltaic and fluvial deposits of upper Eocene to lower Oligocene Enping Formation (Fig. 2). Moreover, during the deposition of middle Eocene Wenchang Formation, independent sub-sags of the northern PRMB were separated by uplifts where subaqueous fans and fan deltas developed on the steep slope and braided deltas on the gentle slope (Shi et al., 2009; Wang et al., 2015). During the deposition of upper Eocene to lower Oligocene Enping Formation, there were relatively large braided deltas and fan deltas, but no subaqueous fan (Shi et al., 2009; Wang et al., 2015). During the transitional stage that started since the late Oligocene, the northern SCS experienced the Nanhai event which is featured by significant sea-floor spreading, and accordingly the PRMB evolved into a continental-to-marine environment depositing the upper Oligocene Zhuhai Formation (Taylor and Hayes, 1983; Briais et al., 1993).

2.2. Potential source areas of the Paleogene PRMB

Depending on whether sediment came from internal or external PRMB, the Paleogene PRMB evidently had two main provenance areas: intrabasinal and extrabasinal (Clift et al., 2002, 2015; Hayes and Nissen, 2005; Wang et al., 2017; Cao et al., 2018; Liu et al., 2022). Based on the present geographic framework in the northern continental margin of SCS, two main extrabasinal source areas are defined: the South China Block and the Hainan Island, located to the north and west of PRMB, respectively (Fig. 1).

The South China Block experienced three main periods of Phanerozoic tectonic movement, including Kwangsian (465–400 Ma), Indosinian (270–195 Ma), and Yanshanian (180–90 Ma) orogenies (Li et al., 2006; Zhou et al., 2006; Wang et al., 2011, 2013). The Kwangsian orogeny is commonly thought as intracontinental collision during the early Paleozoic (Wang et al., 2011). The Indosinian orogeny was first defined in the Indochina Block in Vietnam (Lepvrier et al., 2004) and is closely related to the Triassic thermotectonic event in the South China Block; furthermore, associated igneous activity and metamorphism are very common in the South China Block (Carter and Clift, 2008; Wang et al., 2013). As for the Yanshanian orogeny, it caused widespread magmatism and metamorphism from Jurassic to Cretaceous (Zhou

et al., 2006). In response to these tectonic events, one of the largest granite provinces in the world was formed as a result of extensive Phanerozoic igneous rock intrusion to the east of the Anhua–Luocheng fault (fault 1 in Fig. 1) (Zhou et al., 2006; Wang et al., 2011). In the southeast of the South China Block, the Zhenghe–Dapu fault (fault 3 in Fig. 1) separates Cretaceous volcanic rocks and granites to the southeast and pre-Cretaceous granites to the northwest (Xu et al., 2007). In addition, Precambrian metamorphic and magmatic rocks, including those from the Jinningian (1000–750 Ma) orogeny, are widely found in the South China Block (Li et al., 2003). The Jiangshan–Shaoxing fault (fault 2 in Fig. 1) sutures the South China Block, which is made up of the Cathaysia Block to the southeast and the Yangtze Block to the northwest (Guo et al., 1989; Li et al., 2009; Wang et al., 2013; Yao et al., 2013). The Pearl River is a significant drainage system that flows from the South China Block into SCS. Studies on zircon geochronology of Pearl River sands provide unique perspective on the age of the South China Block (Xu et al., 2007; Zhao et al., 2015; Liu et al., 2017). The Pearl River consists of northeastern tributaries and western tributaries; the former flow mainly through the Cathaysia Block entraining sediments with a major zircon U–Pb age peak at ca. 159 Ma and minor zircon U–Pb age peaks at ca. 239 Ma, ca. 451 Ma and ca. 946 Ma (Fig. 3A) (Xu et al., 2007; Liu et al., 2017). By contrast, the western tributaries flow mainly through the Yangtze Block entraining sediments with a major zircon U–Pb age peak at ca. 267 Ma, with less Mesozoic age groups and more Precambrian age groups (Fig. 3B) (Liu et al., 2017).

In addition to the South China Block in the north of PRMB, the sediments may also derive from Hainan Island, to the west of PRMB. Hainan Island is thought to be a part of the South China Block before the Eocene (Chen et al., 2022), which is now separated from it by the Qiongzhou Strait. Hainan Island is occupied by Permian to Mesozoic granitoids, minor Precambrian and Paleozoic metamorphic rocks (Zhao and Cawood, 2012), and by Cretaceous to Eocene sedimentary basins. Zircon U–Pb ages of Permian–Cretaceous granitic rocks (Yan et al., 2017), Cretaceous–Eocene sedimentary rocks (Jiang et al., 2015; Chen et al., 2022) and modern river sands (Xu et al., 2014; Chen et al., 2022) were collected for the age of Hainan Island. The zircon U–Pb age spectrum shows that the Hainan Island is dominated by a major Indosinian peak at ca. 242 Ma and a minor Yanshanian peak at ca. 110 Ma (Fig. 3C) (Xu et al., 2014; Jiang et al., 2015; Yan et al., 2017; Chen et al., 2022).

By contrast, the intrabasinal provenance, i.e. the Mesozoic basement, plays a significant role during the syn-rift stage of PRMB. To the west of the Yangjiang–Yitongansha fault (fault 4 in Fig. 1), the basement of the PRMB is made up of low-grade metamorphic strata, whereas to the east of the Yangjiang–Yitongansha fault (fault 4 in Fig. 1), the basement of the PRMB consists of the Mesozoic igneous and sedimentary rocks (Lu et al., 2011; Wang et al., 2017). In addition, in the northern PRMB,

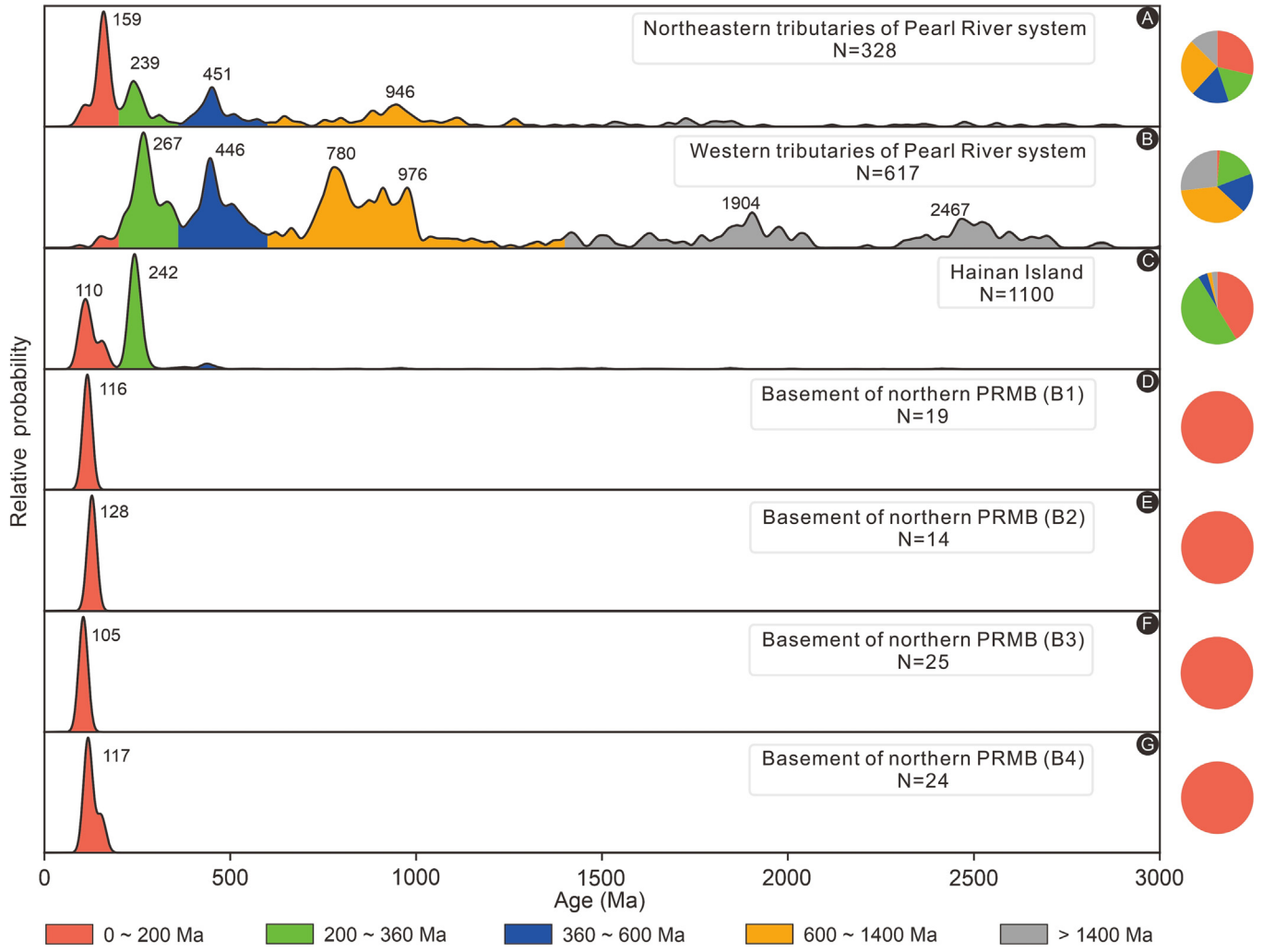

Fig. 3. Compilation of published detrital zircon U–Pb ages from the northern margin of the SCS. U–Pb ages of zircon grains from the western and northeastern tributaries of the Pearl River system (Xu et al., 2007; Liu et al., 2017), the Hainan Island (Xu et al., 2014; Jiang et al., 2015; Yan et al., 2017; Chen et al., 2022), and the basement of northern PRMB (provided by Shenzhen Branch of China National Offshore Oil Corporation Ltd) are shown in the form of kernel density estimation (KDE) plots. Patches with different colors represent different age populations defined in this study. Pie charts indicating the percentage contributions of identified ages are put on the side. N: number of concordant analyses.

Table 1
A summary of samples from northern PRMB analyzed in this study for zircon U–Pb ages.

Location	Borehole	Sample	Depth (m)	Strata	Number of zircon analyses	Reference
Huizhou Sag	H1	H1-LO	3792–3804	Lower Oligocene	98	This study
	H1	H1-UE	4014–4043	Upper Eocene	96	This study
	H2	H2-LO	3873–3889	Lower Oligocene	99	This study
	H3	H3-LO	3454–3473	Lower Oligocene	97	This study
	H3	H3-UE	3669–3682	Upper Eocene	98	This study
	H4	H4-LO	3387–3399	Lower Oligocene	98	This study
	H4	H4-ME	3756–3773	Middle Eocene	96	This study
	H5	H5-LO	3569–3595	Lower Oligocene	98	This study
	H6	H6-UE	3597–3613	Upper Eocene	98	This study
	H6	H6-ME	3942–3958	Middle Eocene	95	This study
	H7	H7-LO	3598–3620	Lower Oligocene	96	This study
	H7	H7-UE	3897–3911	Upper Eocene	86	This study
	H8	H8-LO	3147–3177	Lower Oligocene	90	This study
Xijiang Sag	ZI-5	ZI-5-LM	2392–2825	Lower Miocene	166	Shao et al., 2019
	ZI-5	ZI-5-UO	3391–3425	Upper Oligocene	101	Shao et al., 2016
Dongsha Uplift	B1	B1	2810–2825	pre-Cenozoic	19	CNOOC, 2016
	B2	B2	2217	pre-Cenozoic	14	CNOOC, 2016
Huizhou Sag	B3	B3	4255–4265	pre-Cenozoic	25	CNOOC, 2016
Northern Uplift	B4	B4	2123	pre-Cenozoic	24	CNOOC, 2016

there are several local basement highs, such as the Northern Uplift and the Dongsha Uplift, which are composed mainly of Mesozoic igneous rocks (Li et al., 1998; Shi et al., 2011; Wang et al., 2018). The zircon U–Pb age spectra of four Mesozoic igneous samples (B1 and B2 from Dongsha Uplift, B3 from Northern Uplift and B4 from Huizhou Sag) (Fig. 1), provided by China National Offshore Oil Corporation (CNOOC), are characterized by a single Yanshanian peak age with almost no old-age populations (>200 Ma) in their overall U–Pb age distribution (Fig. 3D, E, F and G). Moreover, volcanic activity within PRMB, caused by Cenozoic tectonic events, produced a significant sediment contribution to the Paleogene succession (Hui et al., 2016; Shi et al., 2020; Wang et al., 2020).

3. Data and methods

3.1. Samples

In this study, a total of 13 fresh Paleogene samples from eight boreholes in Huizhou Sag, northern PRMB were collected for detrital zircon studies, and about 1 kg of sandstones from each sample was used to obtain zircon samples (Table 1). For the middle Eocene, upper Eocene, and lower Oligocene strata, there are respectively two (H4-ME and H6-ME), four (H1-UE, H3-UE, H6-UE and H7-UE), and seven (H1-LO, H2-LO, H3-LO, H4-LO, H5-LO, H7-LO and H8-LO) samples (Fig. 2). Moreover, to obtain the detrital zircon signals of extrabasinal provenance in late Oligocene and early Miocene, two samples of ZI-5-UO and ZI-5-LM in Xijiang Sag were collected (Shao et al., 2016, 2019). Locations of all these samples from depositional sinks are shown in Fig. 1 and Table 1.

For the U–Pb ages of potential source areas, the Shenzhen Branch of CNOOC provided detrital zircon U–Pb age spectra of the intrabasinal provenance, i.e. the Mesozoic magmatic basement of northern PRMB. The associated samples are B1, B2, B3 and B4, all of which are shown in Fig. 1 and Table 1. Moreover, for the northeastern tributaries, western tributaries of the Pearl River system, and Hainan Island, five samples, six samples, and 20 samples, respectively, were used from previous studies, which are also shown in Table 2.

3.2. Detrital zircon geochronology

As an ideal provenance tracer with strong resistance to physical and chemical weathering, zircon can record the original provenance information under different weathering and hydrodynamic transport conditions (Fedo et al., 2003; Lawton, 2014; Blum and Pecha, 2014). Cathodoluminescence (CL) images were employed to recognize the zoning of zircon grains and to select the spot for trace element analyses as well as U–Pb dating. Zircon trace element analyses and U–Pb dating were conducted synchronously by laser ablation-inductively coupled plasma-mass spectrometry (LA-ICP-MS) at Wuhan Sample Solution Analytical Technology Co., Ltd. A Geo-Las Pro laser ablation system and an Agilent 7700e ICP-MS instrument were both used in the LA-ICP-MS analysis. Prior to entering the ICP, helium and argon were combined via a T-connector to serve as the carrier gas and make-up gas, respectively. In the LA-ICP-MS analysis, the spot size was set to be 32 μm and the frequency of the laser was set to be 5 Hz. As external standards, the zircon 91500 and glass NIST610 were employed for U–Pb dating and trace element calibration, respectively (Wiedenbeck et al., 1995; Jochum et al., 2011). The software ICPMSDataCal, which is based on Excel, was used to calculate the U–Th–Pb isotopic ratios (Liu et al., 2010). Each detrital zircon sample had a total of 100 grains analyzed, and the ages were provided with 1σ level of uncertainty. The best age of zircon U–Pb dating was extracted from $^{206}Pb/^{238}U$ or $^{207}Pb/^{206}Pb$ age when the zircon was younger or older than 1000 Ma, respectively. In the meantime, zircon grains with >10 % age discordance would be discarded (Compston et al., 1992). Data were visualized as KDE and CAD using the Python-based detritalPy program (Vermeesch, 2012; Sharman et al., 2018). The Kolmogorov–Smirnov test-based MDS was employed to statistically evaluate the relative dissimilarities of multi-sample age signatures (Vermeesch, 2013).

Table 2
A summary of samples from extrabasinal source areas for zircon U–Pb ages.

Location	Samples	Number of zircon analyses	Reference
Northeastern tributaries of the Pearl River system	S20, S21, SY01	124	Xu et al., 2007
	P1, P4	204	Liu et al., 2017
Western tributaries of the Pearl River system	5, 102, 105, 304, 903, 906	617	Liu et al., 2017
Hainan Island	SY1	93	Xu et al., 2014
	12HN87, NH103	189	Jiang et al., 2015
	LD15, LS15, SL15-1, SL15-2, SY15, WZS15, BT15, JF15, JF15-1, JS15	211	Yan et al., 2017
	K005, PM1-bb-1, PM1-bb-3, PM2-bb-2, PM3-bb-1, PM3-bb-3, NY-02	607	Chen et al., 2022

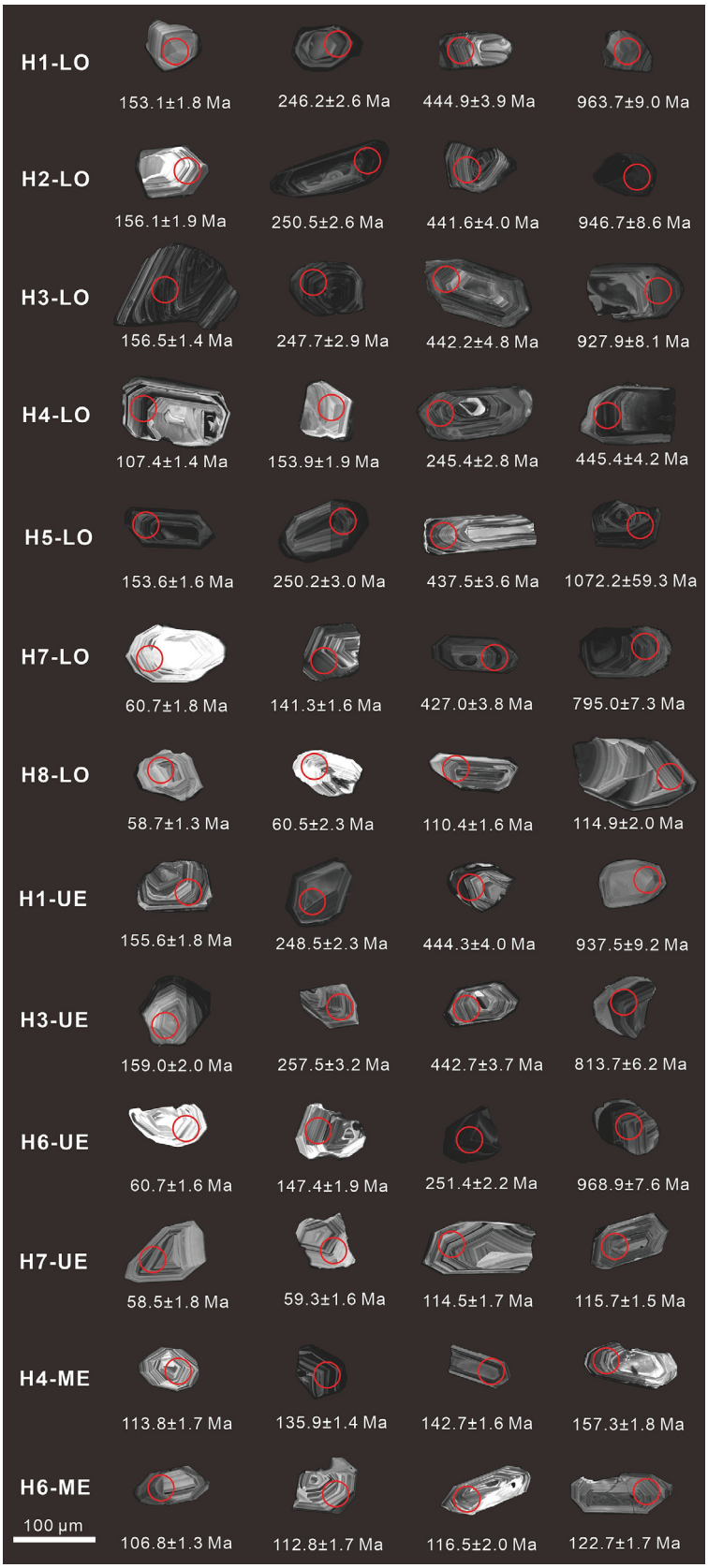

Fig. 4. Cathodoluminescence (CL) images of representative zircon grains from the Paleogene PRMB. The analytical spots are marked by red circles and the associated U–Pb ages are labeled below.

3.3. Crustal thickness analysis

Based on the Eu/Eu^*_{zircon} (chondrite normalized $Eu/\sqrt{(Sm \times Gd)}$) anomaly in detrital zircon, an empirical equation of $(84.2 \pm 9.2) \times Eu/Eu^*_{zircon} + (24.5 \pm 3.3)$ has been used to calculate the crustal thickness, which provides a new insight into the evolution of crustal thickness (Tang et al., 2021). Trace element analysis of 13 detrital zircon samples was conducted on the same spots used for U–Pb dating. Zircon grains with Th/U <0.1 and/or La >1 ppm were discarded to exclude the metamorphic zircons and the data affected by inclusions. The age-binned average crustal thickness was visualized as histogram with each 5 My-interval to indicate the evolutionary history of crustal thickness.

4. Results

4.1. Detrital zircon U–Pb dating

The CL images of representative zircon grains from 13 Paleogene samples in the northern PRMB are shown in Fig. 4. The analytical spots, dated U–Pb ages, and zircon grains exhibiting oscillatory zoning are all presented. As seen in the plot of Th/U ratios versus detrital zircon U–Pb ages in Fig. 5, the Th/U ratios of a total of 1245 zircon grains have a range of 0.01–5.21, among which most zircon grains show high Th/U ratios of >0.3 but few zircon grains show low Th/U ratios of <0.1. As for the U–Pb age distribution, 1245 zircon grains have a wide range of 41–2968 Ma, among which 191 zircon grains from the middle Eocene samples are featured by major Yanshanian U–Pb ages (180–90 Ma) with almost no old-age populations (>200 Ma) in its overall U–Pb pattern. 378 zircon grains from the upper Eocene samples, however, show a multimodal pattern of Yanshanian, Indosinian (270–195 Ma), Kwangsian (465–400 Ma), and several Proterozoic ages. For 676 zircon grains from the lower Oligocene samples, they exhibit a similar U–Pb age pattern to the upper Eocene samples but are featured by a larger proportion of old-age populations (>200 Ma). All these zircon U–Pb ages of 13 fresh samples are listed in Table S1.

The U–Pb ages of 13 detrital zircon samples are plotted as KDE in Fig. 6 to visually display the age populations and highlight the different age distributions.

4.1.1. Middle Eocene

For two middle Eocene samples of H4-ME and H6-ME, the CL images of representative zircon grains shown in Fig. 4 are characterized by obvious oscillatory zoning. For the Th/U ratios versus detrital zircon U–Pb ages, a total of 191 zircon grains from middle Eocene samples have a range of 0.20–2.01, with the age from 41 Ma to 899 Ma (Fig. 5). For the detrital zircon U–Pb age spectra, both of those two samples show the single Yanshanian age peak, which are respectively at ca. 142 Ma (Fig. 6L) and ca. 116 Ma (Fig. 6M).

4.1.2. Upper Eocene

About the four upper Eocene samples H1-UE, H3-UE, H6-UE and H7-UE, the CL images of representative zircon grains derived from samples H3-UE, H6-UE and H7-ME show obvious oscillatory zoning, whereas a Proterozoic grain from sample H1-UE exhibits indistinguishable oscillatory zoning (Fig. 4). The Th/U ratios of a total of 378 zircon grains from the upper Eocene samples have a range of 0.01–2.41, with the age from 42 Ma to 2707 Ma (Fig. 5). As for detrital zircon U–Pb age spectra,

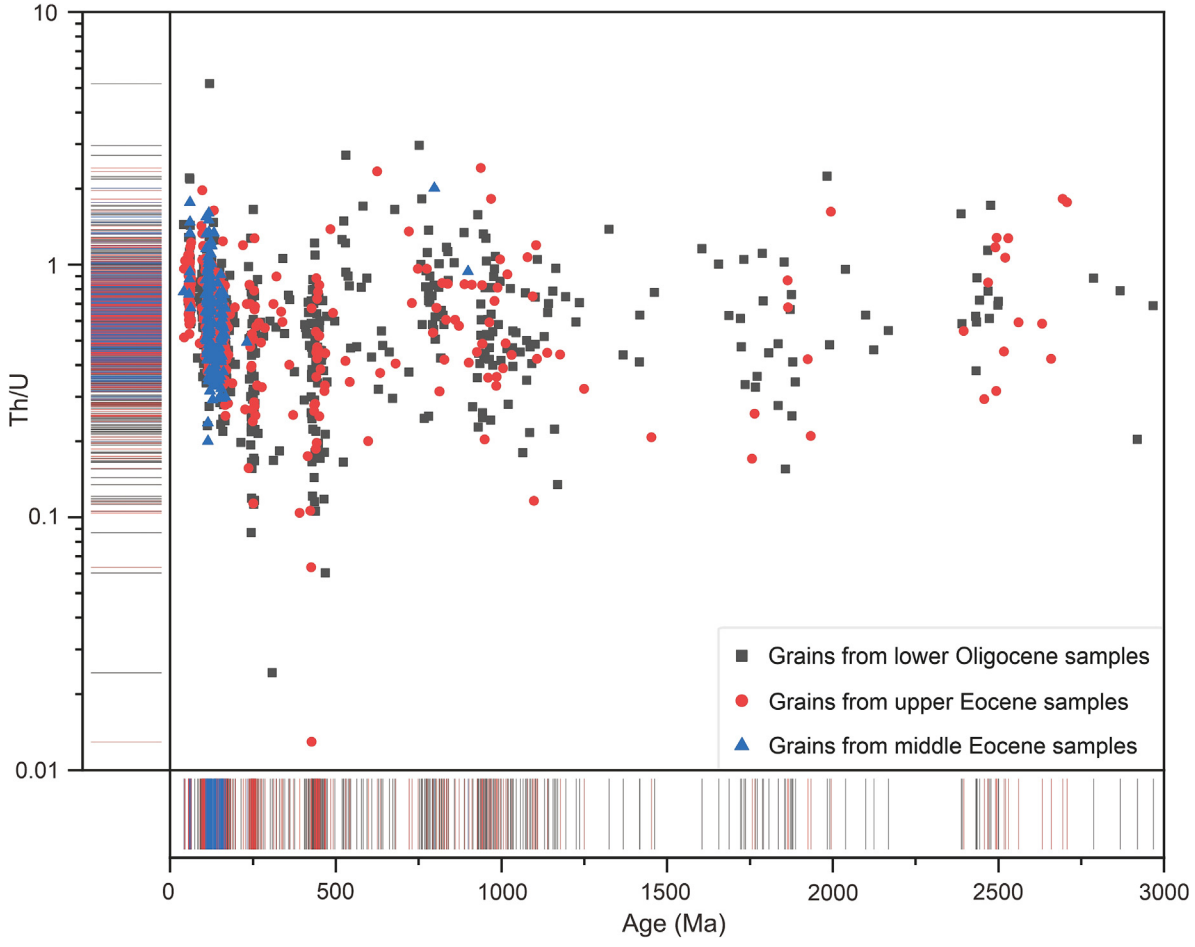

Fig. 5. Plot of Th/U ratios versus U–Pb ages of detrital zircons from all 13 samples in the Paleogene PRMB.

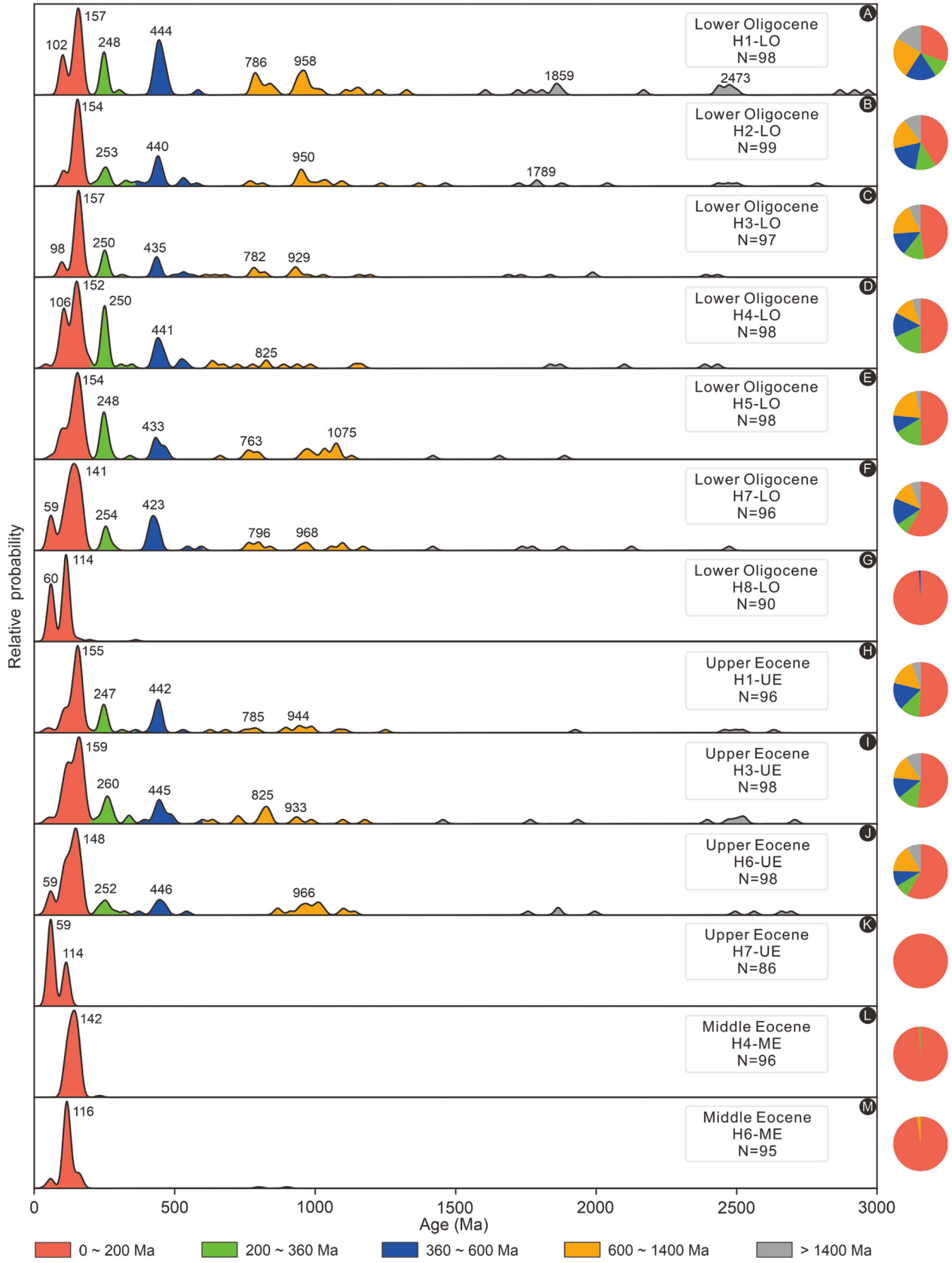

Fig. 6. KDE plots of the detrital zircon U–Pb ages spectra of 13 samples in the Paleogene PRMB. Patches with different colors represent different age populations defined in this study. Pie charts indicating the percentage contributions of identified ages are put on the side. N: number of concordant analyses.

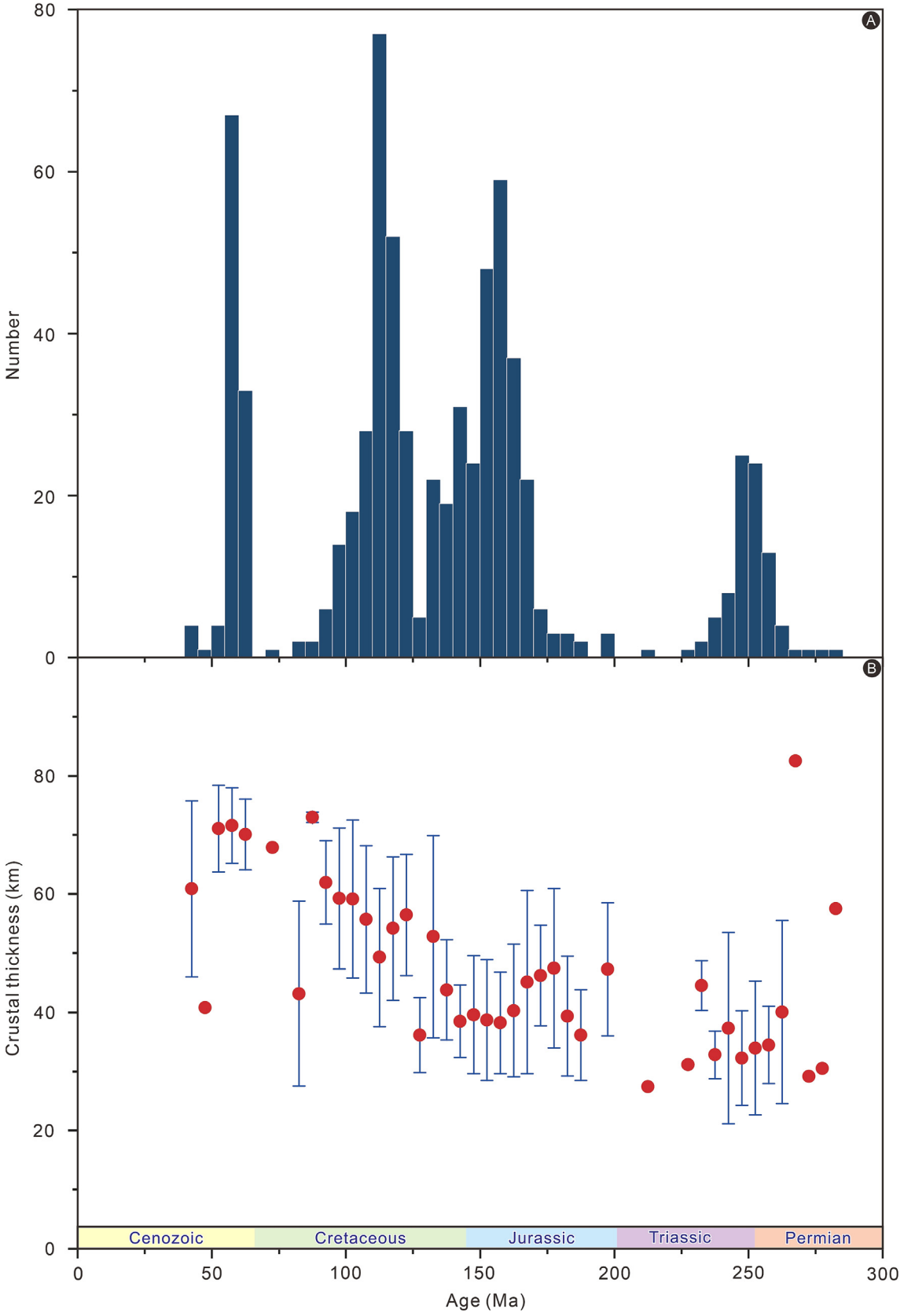

Fig. 7. (A) Age distribution of detrital zircons analyzed for crustal thickness. (B) Changes of crustal thickness of the South China margin through time. Those thickness are calculated from Eu/Eu* in detrital zircons (Tang et al., 2021). Note that the calculated results are plotted as binned averages for every 5 My interval with two standard errors.

sample H7-UE exhibits strong age peaks at ca. 59 Ma and ca. 114 Ma (Fig. 6K). Samples H1-UE, H3-UE and H6-UE, however, show significant differences; besides the major Yanshanian peak, wide age spectra representing Indosinian, Kwangsian and small Jinningian (1000–750 Ma) populations are also found (Fig. 6H, I and J).

4.1.3. Lower Oligocene

For seven lower Oligocene samples (H1-LO, H2-LO, H3-LO, H4-LO, H5-LO, H7-LO and H8-LO), they are sampled from a series of boreholes from northwest to southeast of the Huizhou Sag. The Yanshanian, Indosinian and Kwangsian zircon grains from these samples exhibit obvious oscillatory zoning, whereas the Proterozoic grains show indistinguishable oscillatory zoning (Fig. 4). The Th/U ratios of a total of 676 zircon grains have a range of 0.02–5.21, with the age from 41 Ma to 2968 Ma (Fig. 5). In the southeast of Huizhou Sag, the zircon U–Pb age spectrum of sample H8-LO is featured by bimodal peaks at ca. 60 Ma and ca. 114 Ma (Fig. 6G). To the north, samples H5-LO and H7-LO are characterized by the Yanshanian peak with Indosinian, Kwangsian and Jinningian populations (Fig. 6E and F). Further to the northwest, samples H4-LO, H3-LO, H2-LO and H1-LO are closer to the mouth of the paleo-Pearl River; their zircon U–Pb spectra share the similar distributions to samples H5-LO and H7-LO but have a larger proportion of old-age populations (>200 Ma) (Figs. 1, 6A, B, C and D).

4.2. Crustal thickness

After filtering out those detrital zircon grains with Th/U < 0.1 and/or La > 1 ppm, we totally obtained 708 zircon grains (younger than 300 Ma) from 13 zircon samples to estimate crustal thickness since the Permian (from ca. 300 Ma onwards) (Table S2). The U–Pb ages of these grains range from ca. 282 Ma to ca. 41 Ma and exhibit the major peak at ca. 113 Ma with minor distributions around 58 Ma, 157 Ma or 248 Ma (Fig. 7A). Although zircon grains with Th/U <0.1 and/or La >1 ppm have been discarded to exclude the metamorphic zircons and the data affected by inclusions, there are still some outliers where there are too few grains (e.g., only one or two) for the age-binned average crustal thickness. Excluding outliers with few grains, our reconstructed crustal thickness suggests that the South China margin had a crustal thickness of ca. 35 km in the Permian, which then gradually thickened to ca. 45 km in the Early Triassic. The crustal thickness seems to increase during the Early Jurassic and at the end of the Jurassic it showed a slight decreasing trend. However, during the Cretaceous, our reconstructed crustal thickness increased significantly from ca. 40 km to ca. 70 km (Fig. 7B). There seem to have been small fluctuations in crustal thickness before the Cretaceous, whereas during the Cretaceous, it thickened 75 % (30 km), i.e., an important crustal thickening event in the South China margin.

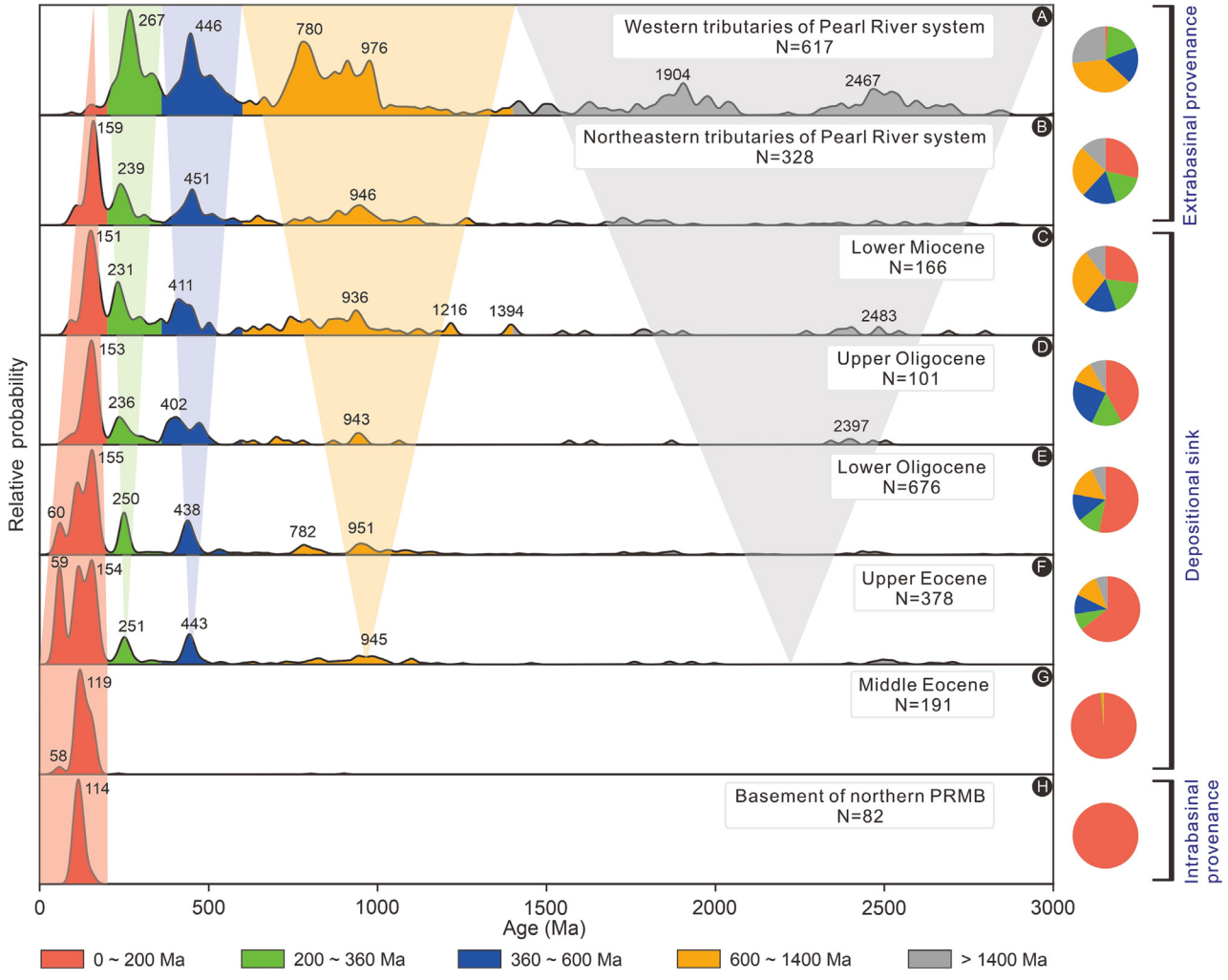

Fig. 8. KDE plots of the detrital zircon U–Pb age spectra of samples from the western (A) and northeastern (B) tributaries of the Pearl River system, the lower Miocene (C), upper Oligocene (D), lower Oligocene (E), upper Eocene (F), middle Eocene (G) successions, and the basement of the northern PRMB (H). Note that different colors represent different age populations and the associated shadowed triangles indicate variation trend of age populations through time. Pie charts on the side indicate the percentage contributions of different age populations defined in this study. N: number of concordant analyses.

5. Discussion

5.1. Provenance change from intrabasinal to extrabasinal

5.1.1. Change in zircon origin from Th/U ratios

The Th/U ratios of zircon grains can be used to reflect the origin of zircon, where high Th/U ratios of >0.3 and low ratios of <0.1 generally indicate the igneous and metamorphic origin, respectively (Möller et al., 2003). In this study, the Th/U ratios of zircon grains from the middle Eocene samples are relatively high, with most values over 0.3 with no values <0.1 (Fig. 5). However, for zircon grains from the upper Eocene and lower Oligocene samples, their Th/U ratios have a wide range of 0.01–5.21 (Fig. 5). Those zircon grains with similar ages from the upper Eocene and lower Oligocene strata have comparable ratios with their counterparts in middle Eocene strata, indicating a similar source for these grains. However, in terms of the age distribution pattern, those grains from upper Eocene and lower Oligocene strata are different from the middle Eocene ones, which show a multimodal distribution pattern and include low Th/U grains. Therefore, it is believed that from the middle Eocene to the late Eocene, there was a change in the origin of zircons.

5.1.2. Provenance change from U–Pb age distributions

Zircon U–Pb geochronology is widely accepted as a reliable tool to reconstruct provenance change (Fedo et al., 2003; Cawood et al., 2012; Cao et al., 2018). By visually comparing the detrital zircon U–Pb age distributions of 13 samples in the northern PRMB and those from samples of potential source areas through KDE, CAD and MDS plots, the provenance of the northern PRMB is traced.

5.1.2.1. KDE plot. As shown in KDE plots of potential source areas and depositional sinks (Figs. 3 and 6), the U–Pb age spectrum with a single Yanshanian peak occurs only in both middle Eocene samples (Fig. 6L and M) and the basement of northern PRMB (Fig. 1D, E, F, and G). The U–Pb age patterns of the upper Eocene to lower Oligocene samples (Fig. 6) are quite different from the U–Pb ages of western tributaries of the Pearl River system without the Yanshanian peak (Fig. 3B), and from the spectrum of Hainan Island with bimodal peaks (Fig. 3C). However, the U–Pb age distributions of the upper Eocene to lower Oligocene samples are similar to the U–Pb ages of northeastern tributaries of the Pearl River system (Fig. 3A), and a complex and wide range of U–Pb ages with a major peak of Yanshanian and three minor peaks of Indosinian, Kwangsian, and Jinningian are clearly shown. Here the zircon U–Pb age spectrum from the Mesozoic basement of northern PRMB is employed as the intrabasinal provenance signal with a limited age distribution (Fig. 8H). In contrast, the zircon U–Pb age spectra from the modern Pearl River system are adopted as the extrabasinal provenance signals of the South China Block with broad age distributions (Fig. 8A and B). As the zircon U–Pb age signatures of modern drainages may not reliably reflect the complex conditions in deep-time, we further plotted samples ZI-5-UO and ZI-5-LM, collected from upper Oligocene and lower Miocene, respectively (Shao et al., 2016, 2019), at borehole ZI-5. These samples from the north of the PRMB are near the mouth of the Pearl River and thus, represent sediments eroded from the South China Block and transported by the paleo-Pearl River. The zircon U–Pb age spectra in Fig. 8 indicate obvious provenance evolution from Eocene to Miocene in northern PRMB. A rapid increase in proportion of old-age populations (>200 Ma) is observed between middle Eocene and upper Eocene strata (Fig. 8F and G), signaling a provenance change from the intrabasinal basement to South China Block occurring between the middle Eocene and the late Eocene.

5.1.2.2. CAD plot. Unlike the KDE plots that exhibit the U–Pb age distribution clearly, the CAD plots are more subtle, and reveal the differences in the proportions of similar ages and the probability growth rate (Sharman et al., 2018). In the CAD plots, the closer the CAD curves are, the greater similarity the U–Pb ages have. As the response to regional thermotectonic events, the rapid growth of CAD curves concentrated mainly in Yanshanian, Indosinian, Kwangsian and Jinningian periods (Fig. 9). For the CAD curves of potential source areas, the Mesozoic basement of northern PRMB has a single segment growth in the Yanshanian period; however, the CAD curve of Hainan Island exhibits a double-segment growth pattern, while the rest show a multi-segment growth pattern. Regarding the CAD curves of depositional sinks, the middle

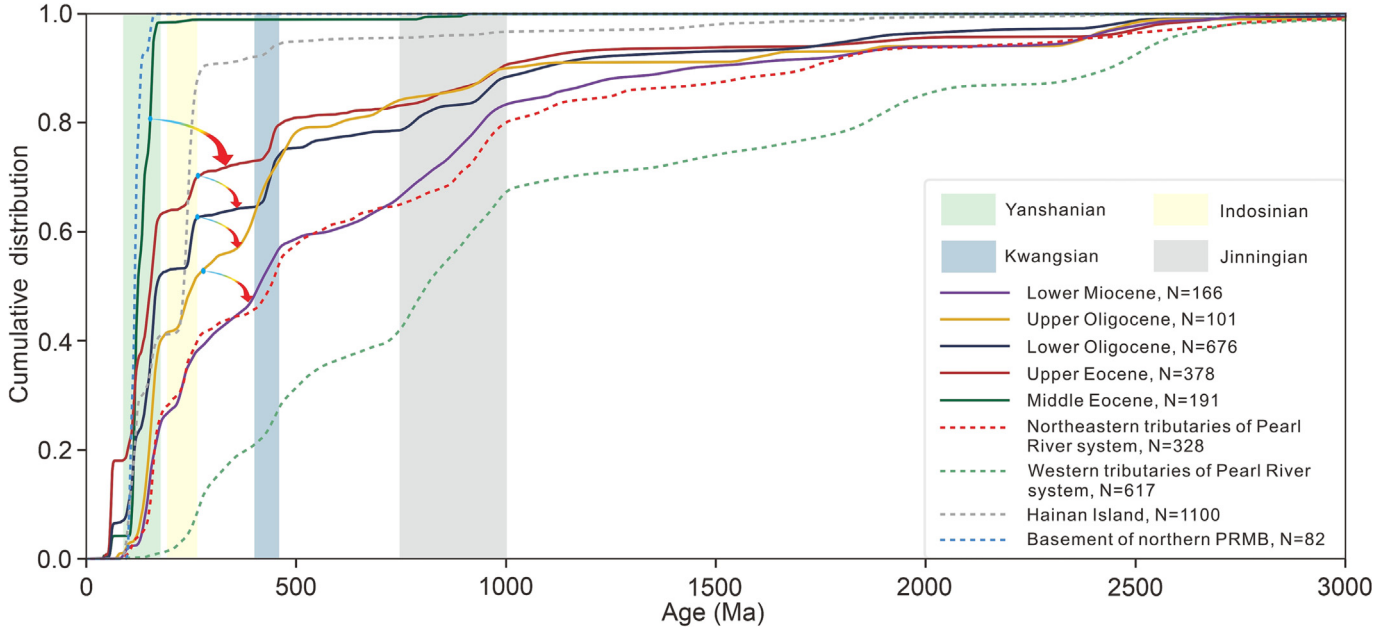

Fig. 9. Cumulative age distribution (CAD) plots of detrital zircon samples from the western and northeastern tributaries of the Pearl River system (Xu et al., 2007; Liu et al., 2017), the Hainan Island (Xu et al., 2014; Jiang et al., 2015; Yan et al., 2017; Chen et al., 2022), the basement of northern PRMB (provided by Shenzhen Branch of China National Offshore Oil Corporation Ltd), and the Cenozoic Xijiang Sag (Shao et al., 2016, 2019) and Huizhou Sag in northern PRMB. Age data from the Paleogene PRMB and potential source areas are respectively shown by solid lines and dotted lines. The colored shadowed bars indicate tectonic-magmatic events in the South China mainland. Yanshanian orogeny: 180– 90 Ma, Indosinian orogeny: 270–195 Ma, Kwangsian orogeny: 465– 400 Ma, Jinningian orogeny: 1000– 750 Ma.

Eocene samples show a growth pattern that is similar to the Mesozoic basement. The CAD curves of sedimentary rocks in northern PRMB, from upper Eocene, through lower Oligocene, to upper Oligocene, are closer and closer to the CAD curve of northeastern tributaries of the Pearl River system. The CAD plots suggest that the middle Eocene PRMB was fed by the Mesozoic basement and the PRMB was fed by the paleo-Pearl River since late Eocene.

5.1.2.3. MDS plot. Further comparison between the zircon U–Pb age distributions within 15 samples of sedimentary rocks in northern PRMB and the defined potential sources is shown by a MDS plot (Fig. 10). The MDS plot separates the samples with different U–Pb age spectra and groups those with similar U–Pb age spectra (Vermeesch, 2013). Zircon U–Pb age spectra with limited Yanshanian distribution from the Mesozoic basement in northern PRMB and samples H4-ME, H6-ME, H7-UE and H8-LO are labeled as Group A. Zircon U–Pb age spectra with major Yanshanian as well as minor Indosinian, Kwangsian, Jinningian distributions, from remaining upper Eocene samples (H1-UE, H3-UE, and H6-UE), the most lower Oligocene samples (H1-LO, H2-LO, H3-LO, H4-LO, H5-LO and H7-LO) and northeastern tributaries of the Pearl River system, are labeled as Group B. Two samples fed by the South China Block are employed to verify the contributions from extrabasinal provenance on northern PRMB, and both samples ZI-5-UO and ZI-5-LM are labeled as Group B in the MDS plot. Zircon U–Pb age spectra of potential provenances from Hainan Island and western tributaries of the Pearl River system that show little similarity to samples from Group A or Group B, are not grouped in this study. As shown in the MDS plot, the two groups indicate two different provenances of PRMB, the Mesozoic basement was the provenance of PRMB during the middle Eocene whereas the South China Block was the main provenance of PRMB since the late Eocene.

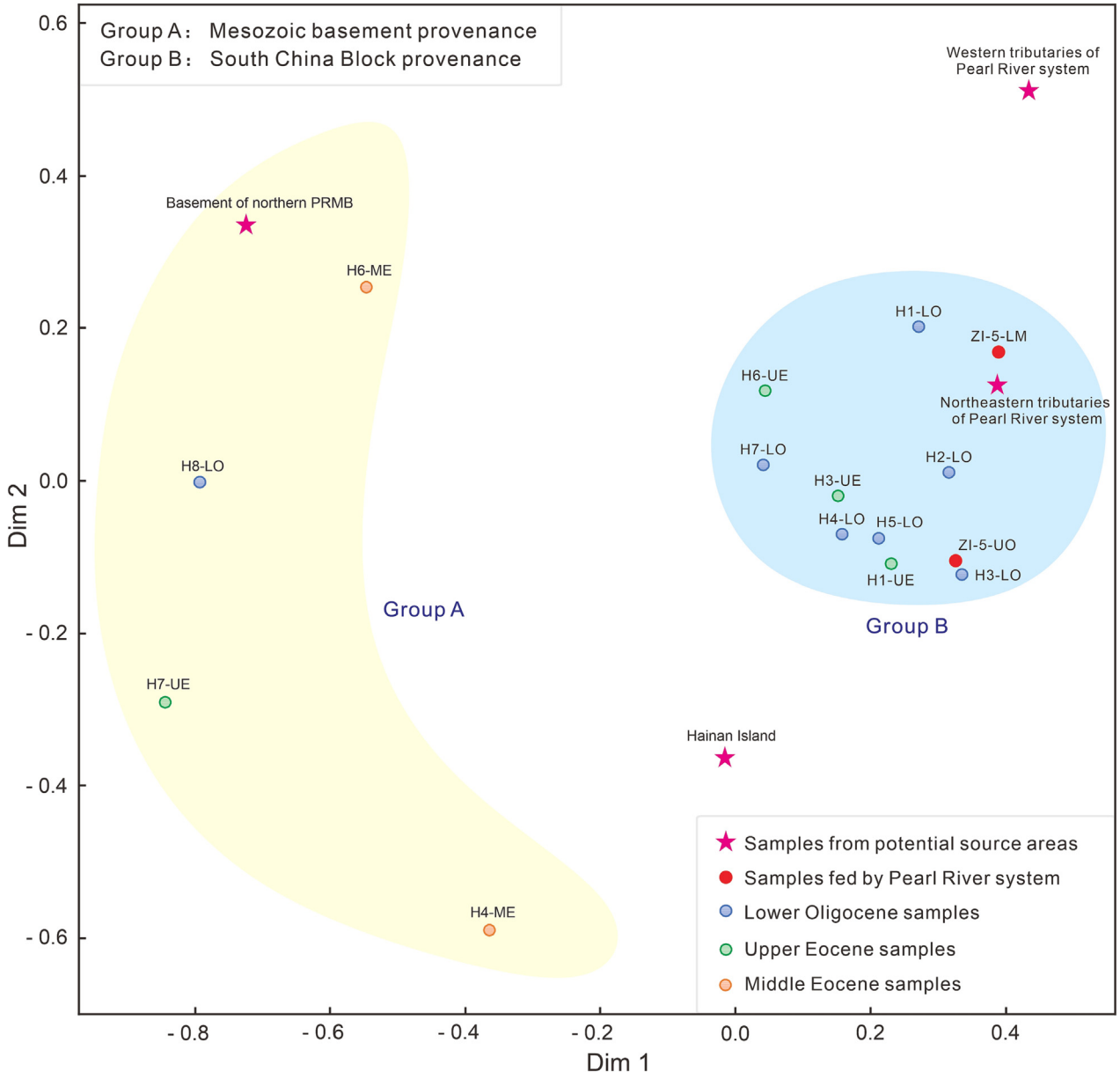

Fig. 10. Multidimensional scaling (MDS) plots of detrital zircon samples from the western and northeastern tributaries of the Pearl River system (Xu et al., 2007; Liu et al., 2017), the Hainan Island (Xu et al., 2014; Jiang et al., 2015; Yan et al., 2017; Chen et al., 2022), the basement of northern PRMB (provided by Shenzhen Branch of China National Offshore Oil Corporation Ltd), and the Cenozoic Xijiang Sag (Shao et al., 2016, 2019) and Huizhou Sag in northern PRMB. The colored shadowed circles indicate samples have a stronger similarity, which in turn are classified as the same groups. Samples fed by Mesozoic basement are labeled as Group A, while samples fed by Cathaysia Block through northeastern tributaries of Pearl River system are labeled as Group B.

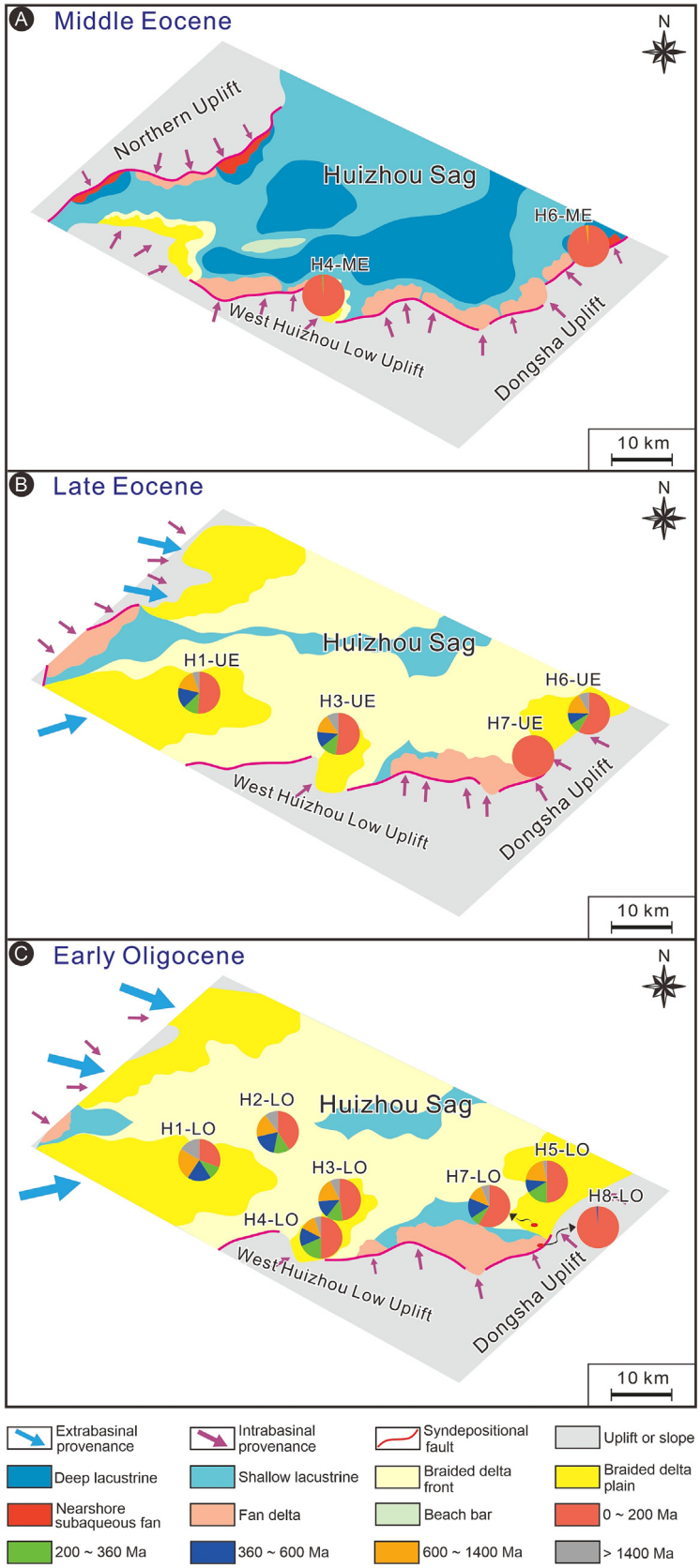

Fig. 11. Detrital zircon U–Pb age patterns of samples from the middle Eocene (A), upper Eocene (B), and lower Oligocene (C) samples, coupled with the map-view depositional facies provided by Shenzhen Branch of China National Offshore Oil Corporation Ltd. Note that the map-view location of depositional facies is marked by the red rectangle in Fig. 1.

Based on the comprehensive visual comparison of KDE, CAD and MDS, we infer that the northern PRMB was fed by two different provenances during the Paleogene. The Hainan Island does not play a significant role in contributing sediments to the northern PRMB. The middle Eocene sediments were primarily contributed by intrabasinal provenance, which were eroded from uplifts and fault blocks of the Mesozoic basement. However, since late Eocene the sediments were primarily transported from the South China Block by northeastern tributaries of the paleo-Pearl River system. A significant provenance change of northern PRMB occurred in the late Eocene.

5.1.3. Depositional response to provenance change

The provenance change plays an important role in the variations of depositional systems, especially in the term of scales. Huizhou Sag, in front of the mouth of the Pearl River, is sensitive to the South China Block provenance. Therefore, the depositional facies diagram of Huizhou Sag provided by the Shenzhen Branch of CNOOC is employed herein to address the linkage between provenance change and sedimentary evolution. In the middle Eocene, contributed by the local uplifts or fault blocks, two samples (H4-ME and H6-ME) located at the southeast Huizhou Sag have a larger proportion of young-age populations (<200 Ma) with almost no old-age populations (>200 Ma) (Fig. 11A). During this period, sediments eroded from the local uplifts or fault blocks on the one side of the syndepositional fault were transported into the steep slope edge along the fault slope break, forming fan deltas or nearshore subaqueous fans with small scales (Shi et al., 2009; Wang et al., 2015; Peng et al., 2016). In the meantime, the limited braided deltas were developed nearby the transfer zones (Tian, 2021).

In the late Eocene, sample H7-UE dominated by the intrabasinal Mesozoic basement provenance shows single young-age populations (<200 Ma), whereas samples H1-UE, H3-UE and H6-UE contributed by the South China Block display complex and wide U–Pb age distributions (Fig. 11B). The influence of South China Block provenance gradually weakened from northwest to southeast while the proportion of old-age populations (>200 Ma) decreases from northwest to southeast Huizhou Sag. During this period, both extrabasinal sediments from the South China Block and those sediments from intrabasinal provenance were transported into depression. Accordingly, the depositional systems were dominated by large braided deltas and limited fan deltas (Shi et al., 2009; Wang et al., 2015; Peng et al., 2016), which have relatively larger scales in the northwest but smaller scales in the southeast.

In boreholes H1, H3 and H7, lower Oligocene samples have relatively larger proportion of old-age populations (>200 Ma) compared with upper Eocene samples, which indicates the enhancement of sediment contribution from the South China Block (Fig. 11C). During this period, the types of developed depositional systems are similar to those occurred in the late Eocene, but they commonly have relative larger scales (Shi et al., 2009; Wang et al., 2015; Peng et al., 2016).

5.2. Paleogeographic pattern that controls provenance change

5.2.1. Uplift of the Coastal Mountains

This study not only pays attention to the observed provenance changes, but also highlights how the regional paleogeographic pattern controls the provenance changes. We have reconstructed the crustal thickness evolution of the South China margin by using Eu/Eu* anomalies in detrital zircons in Fig. 7. The 708 grains generated since 300 Ma from thirteen samples show that there was likely a significant crustal thickness increase from ca. 40 km to ca. 70 km during the Cretaceous. Similar crustal thickening during the Late Mesozoic was found by Eu/Eu* anomalies in detrital zircon from Hainan Island (Chen et al., 2022). This evolution of crustal thickness is compatible with the absolute motion rate of the Izanagi Plate by visual comparison in Fig. 12 (Yang, 2013; Wang et al., 2020; Goldfarb et al., 2021). We thus, infer that the increase of crustal thickness is related to the subduction between the Izanagi Plate and South China Block, referred to here as a Cretaceous orogenic event. As the response to this Cretaceous orogenic event, there was extensive granitoid magmatism and uplift of the Coastal Mountains along the East Asian continental margin, providing a favorable potential source area for PRMB. They are still preserved along the South China coastal areas today though going through considerable erosion after the Cretaceous, such as Yandang Mountain, Wuyi Mountain and Lianhua Mountain (Chen, 1997; Zhang et al., 2016; Tan et al., 2020; Chen et al., 2022).

In this study, a modified paleogeographic pattern is established to explain the relationship between the Cretaceous orogenic event and late Eocene provenance change, a product of the orographic effect and the rain shadow effect of the Coastal Mountains. As the Coastal Mountains uplifted, a topographic high formed along the northwestern South China margin whereas a topographic low formed to the southeast, i.e., the orographic effect. In addition, sedimentary records and simulations in previous studies have suggested that the uplift of the Cretaceous Coastal Mountains resulted in the intensification of aridity in

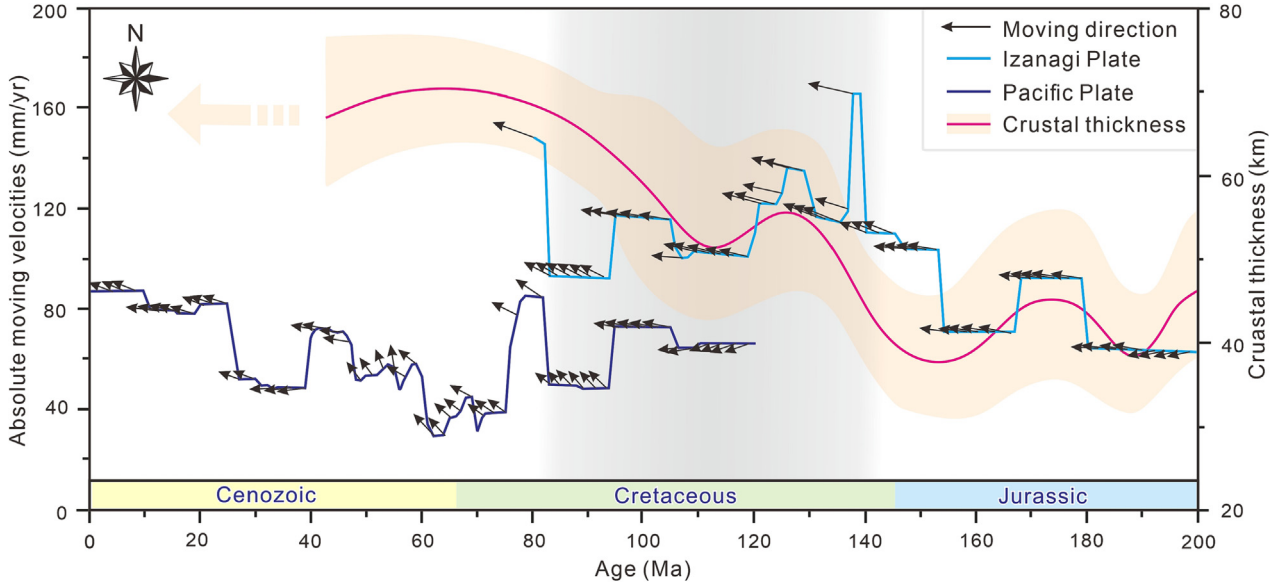

Fig. 12. Changes of crustal thickness and movements of different plates through time on the South China margin. Curves representing the rates and directions of plate movements are from Wang et al. (2020). Colored shadowed zones indicate the standard errors of calculated crustal thickness.

mid-latitude Asia and the formation of typical desert environment in the South China hinterland (Chen, 2000; Cao et al., 2020; Zhang et al., 2021). In contrast, along the southeastern side of the Coastal Mountains, Mesozoic deposition is absent. The semi-humid climate in middle Eocene and humid climate in late Eocene of northern PRMB have been determined by micropaleontological records (Zhang et al., 2020). The Coastal Mountains prevented the humid Pacific air from reaching into the South China hinterland, the rain shadow effect, causing the arid climate in the northwestern side of the Coastal Mountains and relatively humid climate in its southeastern side.

5.2.2. Initiation of the paleo-Pearl River

Similar to the controls of the Tibetan Plateau uplift on the provenance change in the early Miocene, which is through driving the westward expansion of the paleo-Pearl River (Cao et al., 2018; Liu et al., 2022), in this study, we point out that the uplift of the Coastal Mountains controls the late Eocene provenance change of the PRMB from intrabasinal to extrabasinal, through driving the initiation of the paleo-Pearl River. In general, high topographic reliefs and humid climate exhibit more advantages in forming a drainage system. Based on the comprehensive influence of the orographic effect and the rain shadow effect, we infer a linkage between the uplift of the Coastal Mountains and the initiation of the paleo-Pearl River, the most important sediment-routing system of the Paleogene PRMB. The paleo-Pearl River initiated driven by the semi-humid climate as well as the topographic condition during the Late Cretaceous to middle Eocene (Fig. 13A). As the rain shadow effect continued and stacked up, the paleo-Pearl River flowed into PRMB through a long distance since the late Eocene under the humid climate (Fig. 13B). It is

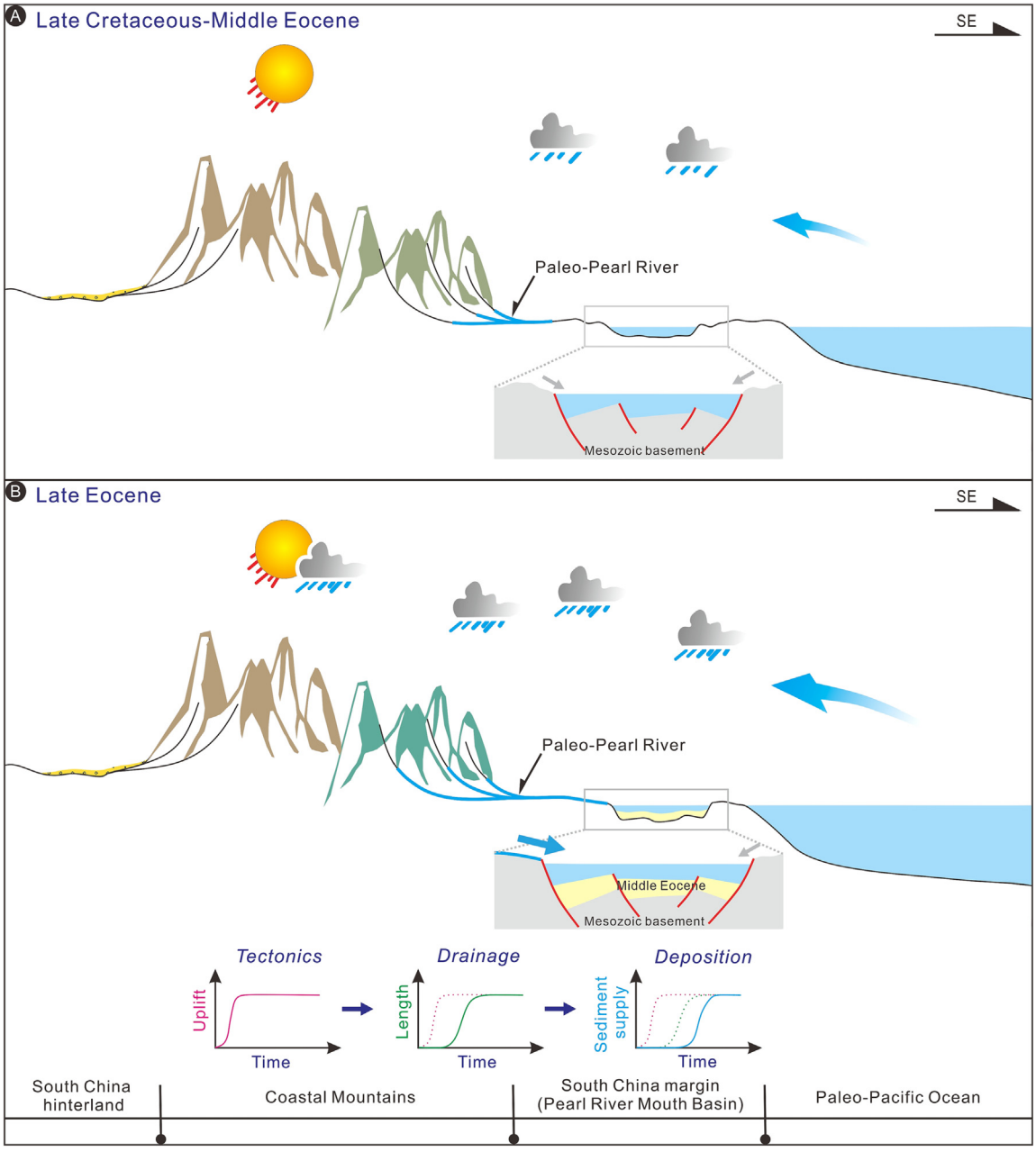

Fig. 13. Paleogeographic patterns along the South China margin from Late Cretaceous-middle Eocene (A) to late Eocene (B). The brown mountains indicate the arid climate, while the celadon and green mountains indicate the semi-humid and humid climates, respectively (modified from Chen, 2000; Cao et al., 2020; Zhang et al., 2020; Zhang et al., 2021). Blue arc arrows show the humid Pacific air directions, and blue solid lines reflect the evolution of the paleo-Pearl River. The structure and provenance of the PRMB are highlighted. The paleo-Pearl River had developed under the effect of Coastal Mountains but had little contribution on the PRMB during the Late Cretaceous-middle Eocene, while the paleo-Pearl River fed the PRMB resulting the provenance change during the late Eocene. Paleogeographic pattern shows the buffered response of provenance change of PRMB to the uplift of Coastal Mountains.

the progressive development of the paleo-Pearl River that resulted in the obvious span from the Late Cretaceous uplift of the Coastal Mountains to the late Eocene entrance of the paleo-Pearl River into the PRMB (Fig. 13). On the one hand, the initiation of the paleo-Pearl River required the overlaying of the rain shadow effect to form a relatively humid climate, which is likely to take a long time. On the other hand, the paleo-Pearl River extended over a long distance from the South China Block to the PRMB, which may also need a long time.

The evolution of the paleo-Pearl River, which is driven by the Cretaceous orogenic event and its resultant uplift of the Coastal Mountains, plays an important role in the provenance change of the PRMB. In the middle Eocene, the paleo-Pearl River had developed flowing from northwest to southeast on a small scale, but had little contribution on northern PRMB, because of the long transport distance from the South China Block to PRMB (Fig. 14A). The zircon U–Pb ages from middle Eocene strata, showing restricted distribution in KDE plots and a single

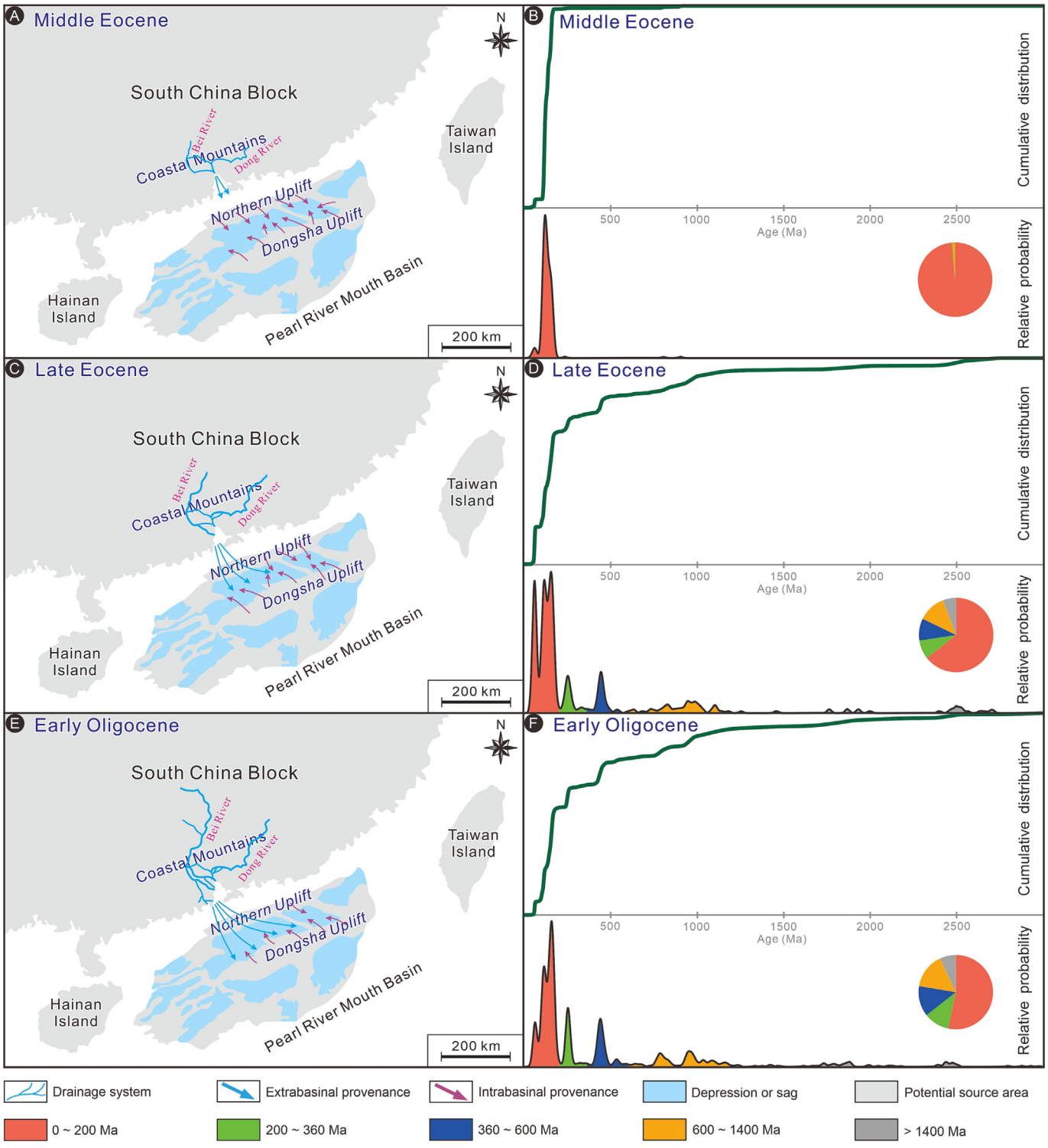

Fig. 14. Sketch diagrams and associated evidences from KDE and CAD plots of detrital zircon U–Pb ages showing the provenance evolution of the northern PRMB from middle Eocene (A–B) through late Eocene (C–D) to early Oligocene (E–F). Also, Pie charts on the side indicate the percentage contributions of different age populations defined in this study. Note that for those sketch diagrams. The purple and blue arrows generally show the provenance directions. Blue solid lines reflect the evolution of regional drainage systems.

segment growth pattern in CAD plots (Fig. 14B), indicate that the middle Eocene PRMB was likely fed by small-catchment streams, sourced from possible intrabasinal uplifts and fault blocks. The absence of old-age populations (>200 Ma) in the U–Pb pattern of middle Eocene samples seems to exclude the sediment fed by the paleo-Pearl River.

In the late Eocene, with the development of drainage through time, the paleo-Pearl River transported abundant sediments through a long transport distance from the South China Block into northern PRMB, resulting in the provenance change from the intrabasinal basement to extrabasinal South China Block (Fig. 14C). A rapid increase in the proportion of old-age populations (>200 Ma) being observed in upper Eocene strata exhibits the contribution of the paleo-Pearl River on northern PRMB since the late Eocene (Fig. 14D). In the early Oligocene, the paleo-Pearl River owning the larger catchment had more contribution on northern PRMB (Fig. 14E). The lower Oligocene strata have a similar zircon U–Pb age distribution with that of the upper Eocene strata, but own larger proportion of old-age populations (>200 Ma), indicating the significant enhancement of the contribution of the paleo-Pearl River on PRMB during this time (Fig. 14F).

6. Conclusions

Zircon U–Pb geochronology analysis from the Paleogene Pearl River Mouth Basin shows a rapid late Eocene increase in the proportion of old-age grains (>200 Ma) in zircon U–Pb age spectra indicating that a provenance change occurred during this time. The middle Eocene sediments were mainly dispersed from an intrabasinal provenance that eroded Mesozoic basement highs, whereas late Eocene sediments were derived mainly from the South China Block by northeastern tributaries of the Pearl River system.

Eu/Eu* anomalies in detrital zircons suggest a significant crustal thickness increase from ca. 40 km to ca. 70 km in the South China margin corresponding to the uplift of the extensive Coastal Mountains in the Late Cretaceous. The uplift of the Coastal Mountains along the South China margin, a Cretaceous orogenic event, caused a favorable potential source area for PRMB. This orogenic event is believed to be related to the subduction between the Izanagi Plate and South China Block during the Cretaceous.

The mechanism of the observed provenance change is revealed from the paleogeographic pattern. The rain shadow effect led to a humid climate in the southeast side of the Coastal Mountains. Strong chemical weathering coupled with the new topographic condition drove the initiation of the paleo-Pearl River during Late Cretaceous to middle Eocene through which sediments were transported into PRMB and in turn, resulting in the late Eocene provenance change from the intrabasinal basement to extrabasinal South China Block.

Supplementary data to this article can be found online at https://doi.org/10.1016/j.sedgeo.2023.106409.

Data availability statement

The data that support the findings of this study are available in the Supporting information of this article.

Declaration of competing interest

We declare that we have no financial and personal relationships with other people or organizations that can inappropriately influence our work.

Acknowledgements

This research was jointly funded by the National Natural Science Foundation of China (No. 41972100) and by the China National Offshore Oil Corporation (No. CCL2020SZPS0168). We thank the Shenzhen Branch of China National Offshore Oil Corporation Ltd for providing borehole samples and geological data from the northern Pearl River Mouth Basin. Insightful and constructive comments from Editor Professor Brian Jones and three reviewers (Dr. Tim Breitfeld, Dr. Abhijit Basu and an anonymous reviewer) are gratefully acknowledged.

References

Allen, P.A., 2008. From landscapes into geological history. Nature 451, 274–276.
Armitage, J.J., Duller, R.A., Whittaker, A.C., Allen, P.A., 2011. Transformation of tectonic and climatic signals from source to sedimentary archive. Nature Geoscience 4, 231–235.
Blum, M., Pecha, M., 2014. Mid-Cretaceous to Paleocene North American drainage reorganization from detrital zircons. Geology 42, 607–610.
Bradley, D.C., O'Sullivan, P., 2017. Detrital zircon geochronology of pre- and syncollisional strata, Acadian orogen, Maine Appalachians. Basin Research 29, 571–590.
Briais, A., Patriat, P., Tapponnier, P., 1993. Updated interpretation of magnetic anomalies and seafloor spreading stages in the South China Sea: implications for the Tertiary tectonics of Southeast Asia. Journal of Geophysical Research 98, 6299–6328.
Brudner, A., Jiang, H., Chu, X., Tang, M., 2022. Crustal thickness of the Grenville orogen: a Mesoproterozoic Tibet? Geology 50, 402–406.
Cao, L., Shao, L., Qiao, P., Zhao, Z., van Hinsbergen, D.J.J., 2018. Early Miocene birth of modern Pearl River recorded low-relief, high-elevation surface formation of SE Tibetan Plateau. Earth and Planetary Science Letters 496, 120–131.
Cao, S., Zhang, L., Wang, C., Ma, J., Tan, J., Zhang, Z., 2020. Sedimentological characteristics and aeolian architecture of a plausible intermountain erg system in Southeast China during the Late Cretaceous. Geological Society of America Bulletin 132, 2475–2488.
Carrapa, B., DeCelles, P.G., Ducea, M.N., Jepson, G., Osakwe, A., Balgord, E., Goddard, A.L.S., Giambiagi, L.A., 2022. Estimates of paleo-crustal thickness at Cerro Aconcagua (Southern Central Andes) from detrital proxy-records: implications for models of continental arc evolution. Earth and Planetary Science Letters 585, 117526.
Carter, A., Clift, P.D., 2008. Was the Indosinian orogeny a Triassic mountain building or a thermotectonic reactivation event? Comptes Rendus Geoscience 340, 83–93.
Carter, L., Orpin, A.R., Kuehl, S.A., 2010. From mountain source to ocean sink–the passage of sediment across an active margin, Waipaoa Sedimentary System, New Zealand. Marine Geology 270, 1–10.
Cawood, P.A., Hawkesworth, C.J., Dhuime, B., 2012. Detrital zircon record and tectonic setting. Geology 40, 875–878.
Chen, P., 1997. Coastal Mountains of SE China, desertization and saliniferous lakes of Central China during the Upper Cretaceous. Journal of Stratigraphy 21, 203–213 (in Chinese with English abstract).
Chen, P., 2000. Paleoenvironmental changes during the Cretaceous in eastern China. Developments in Palaeontology and Stratigraphy 17, 81–90.
Chen, Y., Meng, J., Liu, H., Wang, C., Tang, M., Liu, T., Zhao, Y., 2022. Detrital zircons record the evolution of the Cathaysian Coastal Mountains along the South China margin. Basin Research 34, 688–701.
Clift, P.D., Lee, J.I., Clark, M.K., Blusztajn, J., 2002. Erosional response of South China to arc rifting and monsoonal strengthening; a record from the South China Sea. Marine Geology 184, 207–226.
Clift, P.D., Brune, S., Quinteros, J., 2015. Climate changes control offshore crustal structure at South China Sea continental margin. Earth and Planetary Science Letters 420, 66–72.
Compston, W., Williams, I.S., Kirschvink, J.L., Zhang, Z., Guogan, M.A., 1992. Zircon U–Pb ages for the Early Cambrian time-scale. Journal of the Geological Society 149, 171–184.
Dickinson, W.R., Gehrels, G.E., 2003. U–Pb ages of detrital zircons from Permian and Jurassic eolian sandstones of the Colorado Plateau, USA: paleogeographic implications. Sedimentary Geology 163, 29–66.
Fedo, C.M., Sircombe, K.N., Rainbird, R.H., 2003. Detrital zircon analysis of the sedimentary record. Reviews in Mineralogy and Geochemistry 53, 277–303.
Galloway, W.E., Whiteaker, T.L., Ganey-Curry, P., 2011. History of Cenozoic North American drainage basin evolution, sediment yield, and accumulation in the Gulf of Mexico basin. Geosphere 7, 938–973.
Gilmullina, A., Klausen, T.G., Dore, A.G., Rossi, V.M., Suslova, A., Eide, C.H., 2022. Linking sediment supply variations and tectonic evolution in deep time, source-to-sink systems—the Triassic Greater Barents Sea Basin. Geological Society of America Bulletin 134, 1760–1780.
Goldfarb, R.J., Mao, J., Qiu, K., Goryachev, N., 2021. The great Yanshanian metallogenic event of eastern Asia: consequences from one hundred million years of plate margin geodynamics. Gondwana Research 100, 223–250.
Guo, L., Shi, Y., Lu, H., Ma, R., Dong, H., Yang, S., 1989. The pre-Devonian tectonic patterns and evolution of South China. Journal of Southeast Asian Earth Sciences 3, 87–93.
Hayes, D.E., Nissen, S.S., 2005. The South China sea margins: implications for rifting contrasts. Earth and Planetary Science Letters 237, 601–616.
Hui, G., Li, S., Li, X., Guo, L., Suo, Y., Somerville, I.D., Zhao, S., Hu, M., Lan, H., Zhang, J., 2016. Temporal and spatial distribution of Cenozoic igneous rocks in the South China Sea and its adjacent regions: implications for tectono-magmatic evolution. Geological Journal 51, 429–447.
Jiang, X., Li, X., Collins, W.J., Huang, H., 2015. U–Pb age and Hf–O isotopes of detrital zircons from Hainan Island: implications for Mesozoic subduction models. Lithos 239, 60–70.
Jochum, K.P., Weis, U., Stoll, B., Kuzmin, D., Yang, Q., Raczek, I., Jacob, D.E., Stracke, A., Birbaum, K., Frick, D.A., Günther, D., Enzweiler, J., 2011. Determination of reference values for NIST SRM 610-617 glasses following ISO guidelines. Geostandards and Geoanalytical Research 35, 397–429.
Lawton, T.F., 2014. Small grains, big rivers, continental concepts. Geology 42, 639–640.

Lepvrier, C., Maluski, H., Tich, V.V., Leyreloup, A., Thi, P.T., Vuong, N.V., 2004. The Early Triassic Indosinian orogeny in Vietnam (Truong Son Belt and Kontum Massif); implications for the geodynamic evolution of Indochina. Tectonophysics 393, 87–118.
Li, P., Liang, H., Dai, Y., 1998. Exploration perspective of basement hydrocarbon accumulations in the Pearl River Mouth basin. China Offshore Oil and Gas 12, 361–369 (in Chinese with English abstract).
Li, Z., Li, X., Kinny, P.D., Wang, J., Zhang, S., Zhou, H., 2003. Geochronology of Neoproterozoic syn-rift magmatism in the Yangtze Craton, South China and correlations with other continents: evidence for a mantle superplume that broke up Rodinia. Precambrian Research 122, 85–109.
Li, X., Li, Z., Li, W., Wang, Y., 2006. Initiation of the Indosinian Orogeny in South China: evidence for a Permian Magmatic Arc on Hainan Island. Journal of Geology 114, 341–353.
Li, X., Li, W., Li, Z., Lo, C., Wang, J., Ye, M., Yang, Y., 2009. Amalgamation between the Yangtze and Cathaysia Blocks in South China: constraints from SHRIMP U–Pb zircon ages, geochemistry and Nd–Hf isotopes of the Shuangxiwu volcanic rocks. Precambrian Research 174, 117–128.
Li, J., Dong, S., Cawood, P.A., Zhao, G., Johnston, S.T., Zhang, Y., Xin, Y., 2018. An Andean-type retro-arc foreland system beneath northwest south China revealed by SINOPROBE profiling. Earth and Planetary Science Letters 490, 170–179.
Liu, Y., Gao, S., Hu, Z., Gao, C., Zong, K., Wang, D., 2010. Continental and oceanic crust recycling-induced melt-peridotite interactions in the Trans-North China Orogen: U–Pb dating, Hf isotopes and trace elements in zircons from mantle xenoliths. Journal of Petrology 51, 537–571.
Liu, C., Clift, P.D., Carter, A., Boning, P., Hu, Z., Sun, Z., Pahnke, K., 2017. Controls on modern erosion and the development of the Pearl River drainage in the late Paleogene. Marine Geology 394, 52–68.
Liu, C., Stockli, D.F., Clift, P.D., Wan, S., Stockli, L.D., Hofig, T.W., Schindlbeck-Belo, J.C., 2022. Geochronological and geochemical characterization of paleo-rivers deposits during rifting of the South China Sea. Earth and Planetary Science Letters 584, 117427.
Liu, X., Gao, R., Guo, X., Ding, L., 2023. Detrital zircon U–Pb geochronology of the Lunpola basin strata constrains the Cenozoic tectonic evolution of central Tibet. Gondwana Research 113, 179–193.
Lu, B., Wang, P., Zhang, G., 2011. Basement structures of an epicontinental basin in the northern South China Sea and their significance in petroleum prospect. Acta Petrolei Sinica 32, 580–587 (in Chinese with English abstract).
Ma, M., Chen, G., Lyu, C., Zhang, G., Li, C., Yan, Y., Ma, Z., 2019. The formation and evolution of the paleo-Pearl River and its influence on the source of the northern South China sea. Marine and Petroleum Geology 106, 171–189.
Möller, A., O'Brien, P.J., Kennedy, A., Kröner, A., 2003. Linking growth episodes of zircon and metamorphic textures to zircon chemistry: an example from the ultrahigh-temperature granulites of Rogaland (SW Norway). Geological Society Special Publication 220 (1), 65–81.
Northrup, C.J., Royden, L.H., Burchfiel, B.C., 1995. Motion of the Pacific Plate relative to Eurasia and its potential relation to Cenozoic extension along the eastern margin of Eurasia. Geology 23, 719–722.
Peng, J., Pang, X., Shi, H., Peng, H., Xiao, S., Yu, Q., Wu, L., 2016. Hydrocarbon generation and expulsion characteristics of Eocene source rocks in the Huilu area, northern Pearl River Mouth basin, South China Sea: implications for tight oil potential. Marine and Petroleum Geology 72, 463–487.
Shao, L., Cao, L., Pang, X., Jiang, T., Qiao, P., Zhao, M., 2016. Detrital zircon provenance of the Paleogene syn-rift sediments in the northern South China Sea. Geochemistry, Geophysics, Geosystems 17, 255–269.
Shao, L., Cui, Y., Stattegger, K., Zhu, W., Qiao, P., Zhao, Z., 2019. Drainage control of Eocene to Miocene sedimentary records in the southeastern margin of Eurasian Plate. Geological Society of America Bulletin 131, 461–478.
Sharman, G.R., Sharman, J.P., Sylvester, Z., 2018. detritalPy: a Python-based toolset for visualizing and analysing detrital geo-thermochronologic data. Depositional Record 4, 202–215.
Shi, H., Yu, S., Mei, L., Shu, Y., Wu, J., 2009. Features of Paleogene episodic rifting in Huizhou depression in the Pearl River Mouth Basin. Natural Gas Industry 29, 35–37 (in Chinese with English abstract).
Shi, H., Xu, C., Zhou, Z., Ma, C., 2011. Zircon U–Pb dating on granitoids from the northern South China Sea and its geotectonic relevance. Acta Geologica Sinica 85, 1359–1372.
Shi, H., Du, J., Mei, L., Zhang, X., Hao, S., Liu, P., Deng, P., Zhang, Q., 2020. Huizhou Movement and its significance in Pearl River Mouth Basin, China. Petroleum Exploration and Development 47, 447–461.
Tan, J., Zhang, L., Wang, C., Cao, K., Li, X., 2020. Late Cretaceous provenance change in the Jiaolai Basin, East China: implications for paleogeographic evolution of East Asia. Journal of Asian Earth Sciences 194, 104188.
Tang, M., Ji, W., Chu, X., Wu, A., Chen, C., 2021. Reconstructing crustal thickness evolution from europium anomalies in detrital zircons. Geology 49, 76–80.
Taylor, B., Hayes, D.E., 1983. Origin and history of the South China Sea basin. The Tectonic and Geologic Evolution of Southeast Asian Seas and Islands: Part2vol. 27, pp. 23–56.
Tian, L., 2021. Sedimentary-reservoir characteristics under control of transfer model and implications for hydrocarbon exploration in Huizhou Depression, Pearl River Mouth Basin. Earth Science 46, 4043–4056 (in Chinese with English abstract).
Vermeesch, P., 2012. On the visualisation of detrital age distributions. Chemical Geology 312-313, 190–194.
Vermeesch, P., 2013. Multi-sample comparison of detrital age distributions. Chemical Geology 341, 140–146.
Wang, Y., Zhang, A., Fan, W., Zhao, G., Zhang, G., Zhang, Y., Zhang, F., Li, S., 2011. Kwangsian crustal anatexis within the eastern South China Block: geochemical, zircon U–Pb geochronological and Hf isotopic fingerprints from the gneissoid granites of Wugong and Wuyi-Yunkai Domains. Lithos 127, 239–260.
Wang, Y., Fan, W., Zhang, G., Zhang, Y., 2013. Phanerozoic tectonics of the South China Block: key observations and controversies. Gondwana Research 23, 1273–1305.
Wang, W., Ye, J., Yang, X., Shi, H., Shu, Y., Wu, J., 2015. Sediment provenance and depositional response to multistage rifting, Paleogene Huizhou depression, Pearl River Mouth Basin. Earth Science 40, 1061–1071 (in Chinese with English abstract).
Wang, W., Ye, J., Bidgoli, T., Yang, X., Shi, H., Shu, Y., 2017. Using detrital zircon geochronology to constrain Paleogene provenance and its relationship to rifting in the Zhu 1 depression, Pearl River Mouth Basin, South China Sea. Geochemistry, Geophysics, Geosystems 18, 3976–3999.
Wang, C., Wen, S., Liang, X., Shi, H., Liang, X., 2018. Detrital zircon provenance record of the Oligocene Zhuhai Formation in the Pearl River Mouth Basin, northern South China Sea. Marine and Petroleum Geology 98, 448–461.
Wang, W., Yang, X., Bidgoli, T.S., Ye, J., 2019. Detrital zircon geochronology reveals source-to-sink relationships in the Pearl River Mouth Basin, China. Sedimentary Geology 388, 81–98.
Wang, P., Li, S., Suo, Y., Guo, L., Wang, G., Hui, G., Santosh, M., Somerville, I.D., Cao, X., Li, Y., 2020. Plate tectonic control on the formation and tectonic migration of Cenozoic basins in northern margin of the South China Sea. Geoscience Frontiers 11, 1231–1251.
Wiedenbeck, M., Alle, P., Corfu, F., Griffin, W.L., Meier, M., Oberli, F., Quadt, A.V., Roddick, J.C., Spiegel, W., 1995. Three natural zircon standards for U–Th–Pb, Lu–Hf, trace element and REE analyses. Geostandards and Geoanalytical Research 19, 1–23.
Xu, X., O'Reilly, S.Y., Griffin, W.L., Wang, X., Pearson, N.J., He, Z., 2007. The crust of Cathaysia: age, assembly and reworking of two terranes. Precambrian Research 158, 51–78.
Xu, Y., Sun, Q., Cai, G., Yin, X., Chen, J., 2014. The U–Pb ages and Hf isotopes of detrital zircons from Hainan Island, South China: implications for sediment provenance and the crustal evolution. Environmental Earth Sciences 71, 1619–1628.
Yan, Q., Metcalfe, I., Shi, X., 2017. U–Pb isotope geochronology and geochemistry of granites from Hainan Island (northern South China Sea margin): constraints on late Paleozoic–Mesozoic tectonic evolution. Gondwana Research 49, 333–349.
Yang, Y., 2013. An unrecognized major collision of the Okhotomorsk Blockwith East Asia during the Late Cretaceous, constraints on the plate reorganization of the Northwest Pacific. Earth-Science Reviews 126, 96–115.
Yao, J., Shu, L., Santosh, M., Li, J., 2013. Geochronology and Hf isotope of detrital zircons from Precambrian sequences in the eastern Jiangnan Orogen: constraining the assembly of Yangtze and Cathaysia Blocks in South China. Journal of Asian Earth Sciences 74, 225–243.
Yu, H., 1994. Structure, stratigraphy and basin subsidence of Tertiary basins along the Chinese southeastern continental margin. Tectonophysics 235, 63–76.
Zeng, Z., Zhu, H., Yang, X., Zeng, H., Xia, C., Chen, Y., 2019. Using seismic geomorphology and detrital zircon geochronology to constrain provenance evolution and its response of Paleogene Enping Formation in the Baiyun Sag, Pearl River Mouth Basin, South China sea: implications for paleo-Pearl River drainage evolution. Journal of Petroleum Science and Engineering 177, 663–680.
Zhang, L., Wang, C., Cao, K., Wang, Q., Tan, J., Gao, Y., 2016. High elevation of Jiaolai Basin during the Late Cretaceous: implication for the coastal mountains along the East Asian margin. Earth and Planetary Science Letters 456, 112–123.
Zhang, L., Shu, L., Feng, X., Yu, S., Wu, T., 2020. Further discussion on the age assignment of Enping Formation in the Pearl River Mouth Basin. China Offshore Oil and Gas 32, 9–18 (in Chinese with English abstract).
Zhang, J., Liu, Y., Flögel, S., Zhang, T., Wang, C., Fang, X., 2021. Altitude of the East Asian coastal mountains and their influence on Asian climate during early Late Cretaceous. Journal of Geophysical Research. Atmospheres 126, e2020JD034413.
Zhao, G., Cawood, P.A., 2012. Precambrian geology of China. Precambrian Research 222-223, 13–54.
Zhao, M., Shao, L., Qiao, P., 2015. Characteristics of detrital zircon U–Pb geochronology of the Pearl River Sands and its implication on provenances. Journal of Tongji University (Natural Science) 43, 89–97 (in Chinese with English abstract).
Zhou, X., Sun, T., Shen, W., Shu, L., Niu, Y., 2006. Petrogenesis of Mesozoic granitoids and volcanic rocks in South China: a response to tectonic evolution. Episodes 29, 26–33.